

Dynamic Stripes and Resonance in the Superconducting and Normal Phases of $\text{YBa}_2\text{Cu}_3\text{O}_{6.5}$ Ortho-II Superconductor

C. Stock,¹ W. J. L. Buyers,^{2,3} R. Liang,^{4,3} D. Peets,⁴ Z. Tun,² D. Bonn,^{4,3} W. N. Hardy,^{4,3} and R. J. Birgeneau^{1,3}

¹*Department of Physics, University of Toronto, Ontario M5S 1A7, Canada*

²*National Research Council, Chalk River, Ontario, K0J 1J0, Canada*

³*Canadian Institute of Advanced Research, Toronto, Ontario, M5G 1Z8, Canada*

⁴*Physics Department, University of British Columbia, Vancouver, B. C., V6T 2E7, Canada*

(Dated: February 22, 2019)

We describe the relation between spin fluctuations and superconductivity in a highly-ordered sample of $\text{YBa}_2\text{Cu}_3\text{O}_{6.5}$ using both polarized and unpolarized neutron inelastic scattering. The spin susceptibility in the superconducting phase exhibits one-dimensional incommensurate modulations at low-energies, consistent with hydrodynamic stripes. With increasing energy the susceptibility curves upward to a commensurate, intense, well-defined and asymmetric resonance at 33 meV with a precipitous high-energy cutoff. In the normal phase, which we show is gapless, the resonance remains surprisingly strong and persists clearly in \mathbf{Q} scans and energy scans. Its similar asymmetric spectral form above $T_c=59$ K suggests that incoherent superconducting pairing fluctuations are present in the normal state. On cooling the resonance and the stripe modulations grow in well above T_c below a temperature that is comparable to the pseudogap temperature where suppression occurs in local and low-momentum properties. The spectral weight that accrues to the resonance is largely acquired by transfer from suppressed low-energy fluctuations. We find the resonance to be isotropically polarized, consistent with a triplet carrying $\sim 2.6\%$ of the total spectral weight of the Cu spins in the planes.

PACS numbers: 74.72.-h, 75.25.+z, 75.40.Gb

I. INTRODUCTION

Spin fluctuations play a fundamental role in the superconductivity of high-temperature superconductors. Intensive research has spawned a plethora of theories for the interplay between superconductivity and antiferromagnetism but no model is generally accepted for the unusual behavior of the doped planar cuprate superconductors. The search for new phases of matter, especially in the underdoped region, as the boundary with the antiferromagnetic phase is approached, continues to provide stimulus for experiment and theory.¹ Many recent theories for both the normal and superconducting states have made specific predictions for the spin correlations and therefore a detailed and complete study of $\chi''(\mathbf{Q}, \omega)$ is essential to understanding the cuprates.

One of the most interesting properties of the cuprate phase diagram is the existence of a pseudogap phenomenon seen clearly in tunnelling, NMR, transport, and ARPES experiments.² Tunnelling data have evinced clear evidence of a gap-like structure in the density of states well above the onset to superconductivity.³ Some of the cleanest data have come from NMR studies which have found a suppression of both the Knight shift and the relaxation rate $1/T_1T$ in the normal state.^{4,5}

Many theories have been constructed to explain the pseudogap.⁶ Most recently an orbital current or flux phase has been suggested which predicts circulating currents flowing in the copper-oxide planes.^{7,8,9,10} In the static version of the theory¹⁰ a hidden order parameter, called the d-density wave (DDW), condenses at a temperature well above the superconducting transition tem-

perature. Since, the static DDW order would produce a moment, this phase should be directly observable with neutrons as new Bragg peaks, and since orbital currents break an Ising-like symmetry, a gap should exist in the spin excitation spectrum. We have previously found that no new Bragg peaks are observable in the normal phase of the ortho-II ordered $\text{YBa}_2\text{Cu}_3\text{O}_{6.5}$ (YBCO6.5), thus excluding strong DDW order that breaks the symmetry at $\mathbf{Q} = (\pi, \pi)$. We cannot exclude the possibility of broken orbital symmetry at zero wave vector⁸ or the possibility that the orbital currents are primarily dynamic.⁷

Another theory to explain the variety of phases throughout the cuprate phase diagram is the stripe theory. Upon the introduction of charge, this theory predicts the existence of several phases whose structure is analogous to the nematic and smectic phases of liquid crystals.^{11,12,13} In the stripe picture, charge and spins are spatially segregated with the spins forming antiphase domains. In the smectic phase, long-range correlations exist producing incommensurate Bragg peaks. In the nematic phase, the stripes only have orientational order and therefore the antiferromagnetic correlations will be short-ranged. Also, since the ground state of the stripe phase breaks a continuous symmetry there should be no spin-gap. This theory seems to give a good account of the phase diagram of the $\text{La}_{2-x}\text{Sr}_x\text{CuO}_4$ (LSCO or 214)¹⁴ systems which have been studied in great detail. For YBCO_{6.6} Mook *et al*¹⁵ obtained the first evidence for stripes along the b axis. The overall picture in the $\text{YBa}_2\text{Cu}_3\text{O}_{6+x}$ system is still not clear, however, since a complete study as a function of doping has not been completed and, as we will also show, the structure of the

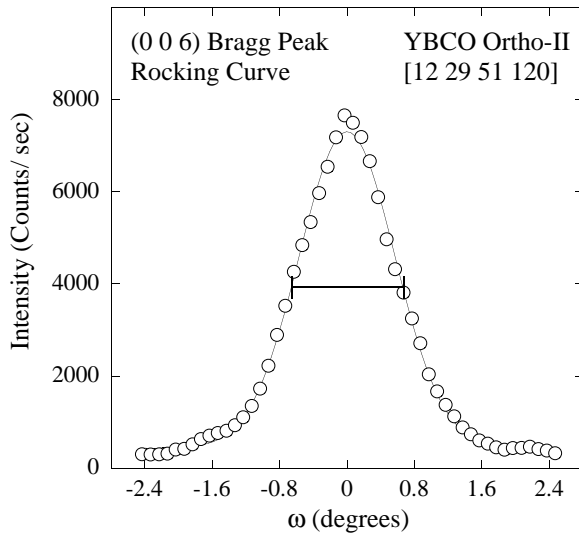


FIG. 1: Rocking curve of the six-crystal composite sample at the (0 0 6) Bragg reflection. The collimation from source to detector is given in minutes of arc within square brackets.

spin dynamics is highly dependent on structural disorder and impurities.

The most striking feature of the spin spectrum in the YBCO_{6+x} system is the presence of an intense resonance peak at low temperatures which is well defined in both momentum and energy.¹⁶ The resonance peak has been observed in the $\text{YBa}_2\text{Cu}_3\text{O}_{6+x}$, $\text{Bi}_2\text{Sr}_2\text{CaCu}_2\text{O}_{8+\delta}$ ¹⁷, and the single layer $\text{Tl}_2\text{Ba}_2\text{CuO}_{6+\delta}$ ¹⁸ systems suggesting that the resonance is a universal feature of all cuprate superconductors. Many theories have been developed to explain the resonance peak in terms of the spin-fermion and band structure models with the Cu^{2+} spins being coupled to the quasiparticles.^{19,20} Since these theories predict that the resonance is a direct consequence of a gap opening in the quasiparticle channel, no well-defined resonance is predicted to exist in the normal phase.

We present a comprehensive high-resolution study of spin fluctuations in the oxygen ordered ortho-II YBCO superconductor in both the normal and superconducting states up to ~ 40 meV energy transfer. The oxygen doping in the system studied $\text{YBCO}_{6.5}$ corresponds²¹ to a hole doping in each CuO_2 plane of $p=0.09$. We expect that the high degree of structural order will remove some of the scattering and dampening seen in the spin response from samples where there is disorder from twinning, poor chain order, and short oxygen chain segments randomly located. We believe that much of the previous discrepancies in the neutron scattering data can be reconciled by the existence of such disorder and a consistent picture of the underdoped region can be formed.

This paper is divided into parts that deal with the normal and superconducting phases. The section on the normal phase will present new results on the temperature dependence of the low-energy excitations that show that no spin gap exists and that one-dimensional incommen-

surate scattering is present that obeys ω/T scaling. In the section on the superconducting phase we show how the low energy scattering is suppressed, and that a resonance peak grows that is much better defined in energy in YBCO ortho-II than it is in disordered YBCO. We end with a discussion of the integrated intensities and the total moment sum rule, where we determine the absolute weight of the resonance in the superconducting phase and the surprisingly large fraction of resonance weight that is already present in the normal phase. Comparisons are made with the pseudogap phenomenon and with theory.

II. EXPERIMENT

The sample consisted of six orthorhombic^{22,23} crystals of total volume $\sim 6 \text{ cm}^3$ aligned on a multi-crystal mount with a combined rocking curve width of $\sim 1.5^\circ$ as shown in Fig. 1. The lattice constants were measured to be $a=3.81 \text{ \AA}$, $b=3.86 \text{ \AA}$, and $c=11.67 \text{ \AA}$. Details of the crystal growth, the detwinning by stress along the a axis and the oxygen order have been given earlier.^{24,25} The (2 0 0) scan of Fig. 2 shows that the majority domain occupies 70% of the sample volume. The peak at larger $|\mathbf{Q}|$ ($H=2$) is the (2 0 0) Bragg peak from the majority squeezed domain, and the peak $H=1.98$ is the (0 2 0) of the minority domain. An independent check is obtained from the satellites produced by oxygen chain order at (3/2 0 0) and (0 3/2 0)(Fig. 3). Fig. 3 shows scans through the oxygen superlattice peaks. Fits to resolution-convolved Lorentzians showed that the oxygen correlation length exceeded $\sim 100 \text{ \AA}$ in the a and b directions, while it was approximately 50 \AA along the c direction. The correlation lengths compare favorably to the x-ray characterization of highly ordered ortho-II indicating the high quality of our crystals.^{26,27}

The measurements were carried out with the DUAL-SPEC triple axis spectrometer at the C5 beam of the NRU reactor at Chalk River Laboratories. A focusing graphite (002) monochromator and a graphite (002) analyzer were used. A pyrolytic graphite filter in the scattered beam eliminated higher order reflections and the final energy was fixed at $E_f = 14.6 \text{ meV}$. For unpolarized measurements the horizontal collimation was set at [33' 29' S 51' 120'] for energy transfer greater than 10 meV and set to [33' 48' S 51' 120'] for energy transfers below 10 meV where the magnetic scattering is weaker. The vertical collimation was kept fixed at [80' 240' S 214' 430']. The six-crystal assembly was mounted in a closed-cycle refrigerator that was carried on an open C-cradle. For constant-energy scans along the in-plane directions the rotation axis of the C cradle was along the [001] direction. This permitted scans along (H H 0) in zones (1/2 1/2 L), and, by rotating the C-cradle by $\sim 26^\circ$, also along (H 3H 0) in the (1/2, 3/2, L) zone. To study the incommensurate nature of the magnetic Q-correlated peaks, scans were made along the [H 0 0], [0 K 0], and [0 0 L] directions independently with respect to the zone

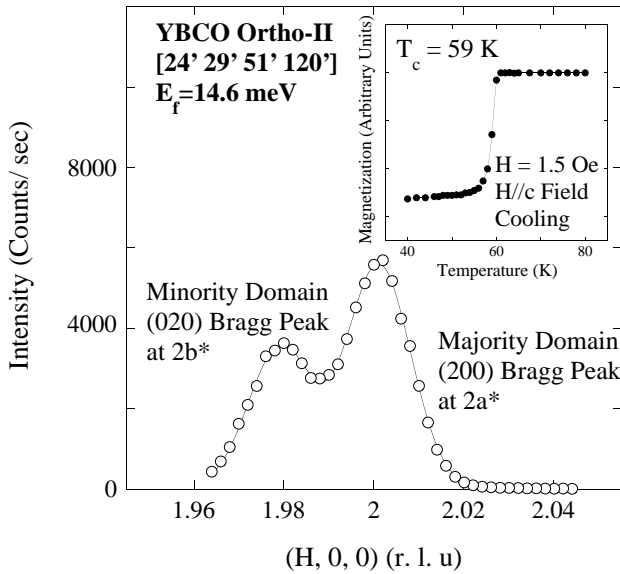


FIG. 2: Radial scan through the (2 0 0) Bragg peak. The Gaussian fit shows that the majority domain occupies 70% of the sample volume. The magnetization inset shows a sharp superconducting transition temperature at 59 K with a width of ~ 2.5 K.

center (1/2, 3/2, L). To do this, the rotation axis of the C-cradle was placed along the $\bar{[1}10]$ direction. By slaving the C-rotation to the L value we could access a general (H K L).

To confirm the magnetic origin of our scattering we made polarized measurements with a Heusler (111) monochromator and analyzer. A flipper coil was placed on the incident side and a graphite filter was used on the scattered side to filter higher order neutrons. A Mezei flipper in the incident beam allowed spin-flip (SF) and non-spin-flip (NSF) cross sections to be measured. At the sample two pairs of coils applied either a weak horizontal (HF) parallel to \mathbf{Q} or vertical field (VF) perpendicular to \mathbf{Q} (of $\sim 3\text{-}5$ gauss) to control the direction of the neutron spin at the sample. With the flipper on, the difference between the HF and VF count rates gives the spin-flip scattering from the magnetic electrons alone independent of nuclear incoherent or phonon scattering.²⁸ To prevent any possible depolarization from the Meissner state the sample was always warmed to 100 K (~ 40 degrees above the transition temperature) and then field cooled to low temperatures. During scans the field direction with respect to the sample never changed more than a few degrees thereby minimizing the effects of depolarization on the neutron beam.

We measured the polarized scattering with two different Heusler analyzers. The first small analyzer, $7.9 \times 3.2 \text{ cm}^2$, was used for the constant energy scans. The horizontal collimation was set to [33' 48' S 126' 120'] and the vertical collimation was [80' 72' S 120' 430']. The second taller analyzer of dimensions $13 \times 12 \text{ cm}^2$ was installed for

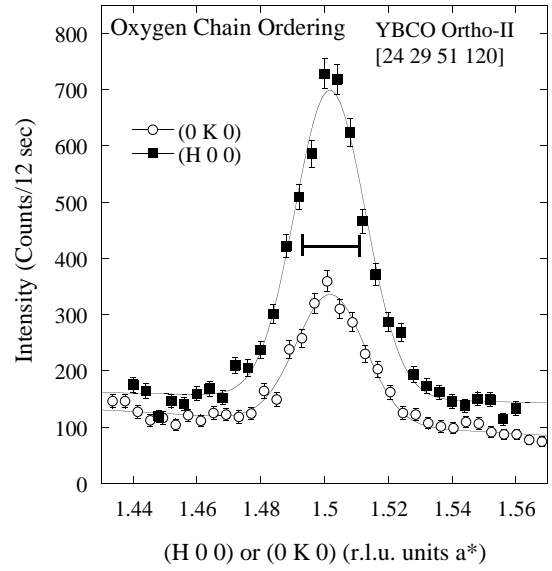


FIG. 3: Radial scans through the oxygen ordering superlattice peaks at (3/2 0 0) and (0 3/2 0) (units of a^*). The horizontal bar indicates the resolution. A fit to a resolution-convolved Lorentzian shows the oxygen ordering correlation length exceeds 100 \AA . The larger peak (filled squares) is from the majority domain and the lesser from the minority domain.

the constant- \mathbf{Q} studies through the resonance. The horizontal collimation was then set to [33' 48' S 126' 120'] and the vertical collimation was [80' 72' S 280' 430']. The flipping ratios from both the small and large analyzer crystals were measured at the (2, 2, 0) Bragg position for $E_i = E_f = 47.6$ meV, the incident energy at the resonance peak. The flipping ratio with the small analyzer was found to be 19:1 for both VF and HF field directions. The flipping ratio for the tall analyzer was measured to be 15:1 for the HF and 12:1 for the VF directions. By using a taller analyzer we were able to obtain a factor of two increase in the resonance scattering per unit time.

To compare our results with those of other groups and to connect with theory we have put our measurements of $\chi''(\mathbf{Q}, \omega)$ on an absolute scale. We have calibrated the spectrometer by measuring the integrated intensity of an acoustic phonon near the strong (0 0 6) Bragg peak. By comparing the measured energy-integrated intensity to that calculated in the long-wavelength limit, where eigenvectors are known, we were able to obtain the calibration constant that puts the magnetic intensities on an absolute scale. Details are provided in the Appendices. The Appendices also show how we made the correction for monitor contamination by higher-order wavelength neutrons. This correction is particularly important at small energies, where its neglect may lead to an underestimate of the low energy response.

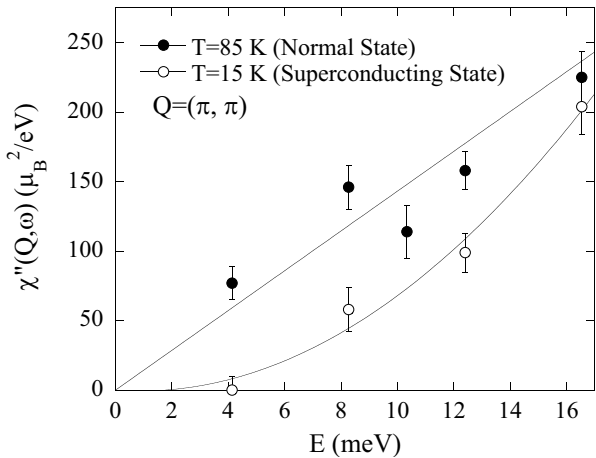


FIG. 4: The peak dynamic susceptibility, χ'' , at $\mathbf{Q} = (\pi, \pi)$ as a function of energy transfer for energies below 16 meV in the normal and superconducting states. In the normal state scattering is present at the lowest energies studied and increases roughly linearly with energy transfer (line). In the superconducting state the scattering is suppressed but not eliminated for energies below 16 meV (the lines are a guides to the eye).

III. THE NORMAL STATE

A. Gapless normal state spin excitations

The existence or not of a normal state spin gap has many important theoretical implications. Theories involving a broken discrete symmetry such as orbital currents require the existence of a normal state spin-gap at low temperature. In one model, the d-density wave (DDW) theory, the orbital currents are equivalent to static weak moments with Ising-like behavior, and the theory predicts that a magnetic Bragg peak will appear in the underdoped phase at temperatures well above the onset temperature of superconductivity.¹⁰ In this model, in which the orbital currents are in opposite directions in adjacent unit cells, the DDW peak is predicted to break the spatial symmetry of the copper oxide plane and to appear at $\mathbf{Q} = (\pi, \pi)$. In the fluctuating orbital current theory of Wen and Lee^{7,9} there is no static order, and there is a crossover to fluctuations that compete with superconducting fluctuations in the normal phase. It is possible that this might still lead to a suppression of the magnetic spectral weight well above T_c .

Experiments on underdoped YBCO in which no observable scattering below ~ 10 meV has been detected have been taken as evidence for a pseudogap phase in the normal state.²⁹ In terms of this interpretation the pseudogap is defined to be a range in energy transfer where there is zero or negligible spectral weight in the energy response as measured by the dynamic susceptibility, $\chi''(\omega)$, and which lies below a range with appreciable weight. Another definition of the pseudogap phase arises

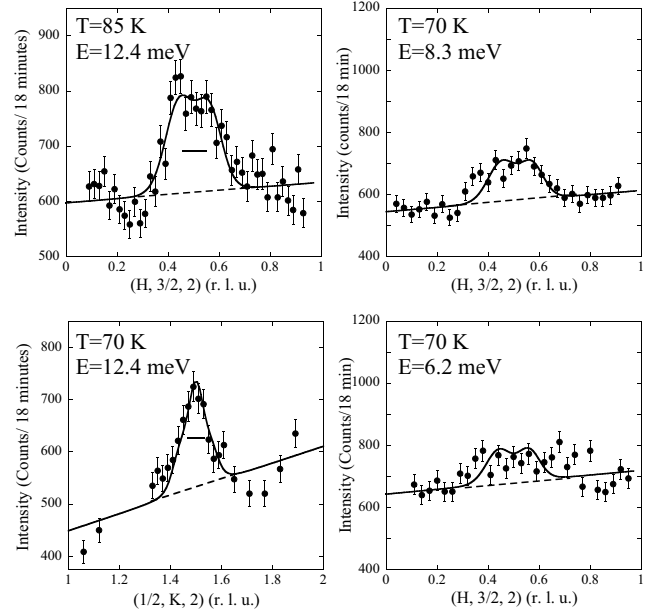


FIG. 5: Normal state neutron scattering scans through $(1/2 \ 3/2 \ 2)$ at energy transfers of 12.4, 8.3, and 6.2 meV. The correction for higher order contamination of the monitor rate has been made. In the left two panels the scattering along $[100]$ reveals incommensurate features, but along $[010]$ it does not (see text). The solid curve is a fit of the spin-wave model of Chou *et al* discussed in the text. Their relative weight is given by the 70:30 domain ratio. The broken lines give the linear background.

from NMR studies which have shown the *suppression*, not absence, of both the Knight shift and the relaxation rate, $1/T_1 T$, well above the superconducting transition temperature.^{2,30,31,32} Based on this we interpret the normal phase pseudogap to be a spectral range in which either there is negligible scattering or there is substantial suppression of the scattering with decreasing temperature. Therefore, in terms of neutron scattering, evidence for a pseudogap must come from both the energy and temperature dependence of χ'' . Recent work on near optimally doped LSCO has shown some evidence for a spin pseudogap based on both the energy and temperature dependence of the scattering.³³ As regards the observed dynamics we find no evidence for a gap or pseudogap in the normal phase of YBCO_{6.5} based on the temperature and energy dependence of χ'' . In this section we present our results on the energy dependence of χ'' pointing to gapless excitations in the normal phase. The temperature dependence showing χ'' increasing in the normal phase with decreasing temperature is presented in later sections.

In an extensive survey of the low-energy spectra we have observed that scattering centered on $\mathbf{Q} = (\pi, \pi)$ clearly exists in the normal state and extends to the lowest energies studied (~ 4 meV). A summary of our results, shown in Fig. 4, indicates the absence of any clear normal state spin pseudogap in contrast to the suggested

behavior by previous studies. The data were obtained by conducting fits to the Q-correlated peak above the background that lies under the magnetic correlations centered on (π, π) . We have removed the temperature-dependent Bose factor and the anisotropic Cu^{2+} form factor from the Q-correlated scattering to obtain the dynamic susceptibility as discussed in detail in the Appendices .

While the spectral weight at low energy is lower than that at the resonance energy (see later), this, in itself, is not sufficient evidence for a gap. We have recently discussed this result in the context of orbital currents and have argued that the presence of low energy excitations is evidence against the presence of a static d-density wave or orbital current phase.²⁵ From Fig. 4 we see that the susceptibility decreases monotonically with energy below ~ 15 meV. The clear suppression of scattering in the superconducting state will be discussed later. Clearly the difficulty of detecting the normal-phase scattering increases at low energies as the weight declines, but the trend is uniform and gives no sign that the spectral response drops off in a way that might suggest a gap. This linear decrease of susceptibility with energy transfer is consistent with over-damped spin waves or fermi liquid behavior. It is also consistent with several early studies of disordered YBCO in the underdoped region.^{34,35,36}

Some typical scans at low energies along the [100] direction through $(1/2 \ 3/2 \ 2)$, are shown in Fig. 5. This zone boundary is equivalent to the 2D wave vector (π, π) with $L=2$ near a maximum of the bilayer structure factor. The results are corrected for the effect of higher order contamination of the monitor rate. If this correction were ignored it would lead to an underestimate of the low-energy intensity by a factor ~ 1.5 at 6 meV as discussed in the Appendices. The solid curves represent the overdamped spin-wave model of Chou *et al.*³⁴ (next section) which gives an excellent fit to the data and also predicts that the scattering should increase roughly proportional to the energy transfer $\hbar\omega$. Because it is more difficult to detect this signal as the energy decreases, it is possible that experiments where the sensitivity and statistics are optimized for the intense resonance peak might have failed to observe the low-energy response and so led to the inference that a gap was present. All of our results indicate that there is no well defined normal state spin-gap in Ortho-II ordered $\text{YBa}_2\text{Cu}_3\text{O}_{6.5}$.

B. Incommensurate dynamic structure in $\text{YBa}_2\text{Cu}_3\text{O}_{6.5}$ Ortho-II

To establish the incommensurate structure we made purely H and K scans (see Fig. 5 left hand panels) in a configuration with good in-plane resolution, where the coarse vertical resolution was only $20\text{-}30^\circ$ from the $(0 \ 0 \ L)$ direction and so did not integrate over the incommensurate peaks. We see that the profile shows incommensurate peaks along a^* but only a commensurate feature along b^* . From the H-K anisotropy of the low-energy

scans in Fig. 5 we can show that the dynamic spin fluctuations are one-dimensional along a^* with an incommensurate wave vector $\delta \sim 0.06$ r.l.u. To do this we recognize that the scattering observed is the sum of that from the majority and minority domains weighted in the oxygen-order ratio of 70:30. Because of the low weight of the incommensurate peaks of the b^* minority domain, the [010] scan shows only a commensurate ridge as the scan passes between the strong a^* peaks at $\pm\delta$ where the resolution picks up its greatest contribution from the wings of the broadened a^* peaks.

Since it gives a good description of the scan profile, we fit the over-damped spin-wave model of Chou *et al.*³⁴ and thereby extract $\delta \sim 0.06$ after convoluting with the spectrometer resolution function. In the Chou model linear branches of damped spin waves rise isotropically in the 2D plane from incommensurate wave vectors displaced by $(\delta, 0)$ in r.l.u. from the AF point $(1/2, 1/2)$, equivalent to $\mathbf{Q}=(\pi, \pi)$ ³⁸. Similar behavior is found for low-energy excitations in the stripe phase of the nickelates³⁷ where the stripes are static instead of fluctuating. As we apply the model to the a^* domain, \mathbf{q} is measured from \mathbf{Q}_0 and the incommensurate wave vector is $\mathbf{q}_{inc} = (\delta, 0, 0)$, so that the Chou model is the sum of scattering from two wave vector origins:

$$S(\mathbf{q}, \omega)|_{\mathbf{q}_{inc}} = A[n(\omega) + 1] \frac{\hbar\omega}{(\kappa^2 + (\mathbf{q} \pm \mathbf{q}_{inc})^2)} \quad (1)$$

$$\times \left(\frac{\Gamma}{(\Gamma^2 + (\hbar\omega - \hbar\omega_{\mathbf{q}\pm})^2)} + \frac{\Gamma}{(\Gamma^2 + (\hbar\omega + \hbar\omega_{\mathbf{q}\pm})^2)} \right),$$

where

$$\hbar\omega_{\mathbf{q}\pm} = \hbar c(\mathbf{q} \pm \mathbf{q}_{inc}) \quad (2)$$

and

$$\Gamma = \hbar c \kappa = \frac{\hbar c}{\xi_0} \quad (3)$$

where c is the spin-wave velocity and ξ_0 can be interpreted as a dynamic correlation length. We emphasize that the parameter ξ_0 is not strictly the instantaneous correlation length as we are not integrating over energy. To account for the minority domain we add to Eq. 1 a similar term in which the scattering emanates from wave vectors $\mathbf{q}_{inc} = (0, \delta, 0)$. Therefore the total cross-section is given as follows:

$$S(\mathbf{q}, \omega) = S(\mathbf{q}, \omega)|_{\mathbf{q}_{inc}=(\delta,0,0)} + R S(\mathbf{q}, \omega)|_{\mathbf{q}_{inc}=(0,\delta,0)}. \quad (4)$$

The ratio of the two amplitudes, R , from the two domains is set to the known domain ratio of 70:30 determined from the oxygen chain superlattice peaks. After folding with the resolution function the fit to the data is performed.

The excellent agreement displayed in Fig. 5 shows that the slow spin correlations are incommensurate in \mathbf{Q} . There is no observable static incommensurate peak. At these low energies, phonon contamination is unlikely and as a check we have verified that the origin of this scattering at each energy transfer is truly magnetic, from its temperature dependence around T_c (see future sections regarding temperature dependence). By iterating through each data set we have chosen the spin-wave velocity, $\hbar c \sim 300$ meV·Å, a dynamic correlation length, $\xi_0 \sim 20$ Å, and incommensurability, $\delta=0.06$, that applies at all energies and temperatures.

As shown in Fig. 5 the fit from this model describes the lineshape along both the [100] and [010] directions very well. The minority domain is not strong enough to be seen as a separate peak in the [010] scan (lower left panel), both because of its small weight and because the majority peaks are broadened by ξ and resolution so that they contribute most of the scattering at the commensurate point $q=0$. Thus the [010] scan shows a single peak at $K=1.5$ as the scan crosses a saddle point between the two majority peaks at $(\pm \delta, 0, 0)$.

Our analysis provides strong evidence that the low-energy spin dynamics reflect a one-dimensional incommensurate structure along a^* . Its dynamics can be associated with the Doppler shift for a right and left moving incommensurate spin density wave. Similar incommensurate scattering has been previously observed for oxygen concentrations of $x = 0.6^{15}$ and $x = 0.7^{39}$ at energies of ~ 20 meV, where the incommensurate wave vector and doping is larger. The one-dimensional incommensurate scattering is thus a common feature of the YBCO_{6+x} system in the underdoped region. One-dimensional incommensurate scattering has also been observed in $\text{La}_{1.95}\text{Sr}_{0.05}\text{CuO}_4^{14}$ indicating that it is possibly a general feature of all cuprates.

Physically, our data can be interpreted in terms of one-dimensional Antiphase domains parallel to the b^* chains. This may be consistent with the stripe picture⁴⁰ in which the spin correlations are antiferromagnetic in a domain between charged walls separated by ℓ spins along [100], where the carriers concentrate. Across a wall the coupling is ferromagnetic so that the next spins belong to an antiphase spin domain π out of phase with the first. A nice feature of the stripe model is that the local spin correlations within a domain remain commensurate, as suggested by analysis of NMR data.⁴¹ Nevertheless, the maximum in a scattering experiment moves away from π to an incommensurate wave vector, $2\pi/2\ell$ i.e., $\delta=1/2\ell$, the inverse of the 2ℓ spin repeat distance for long-ranged stripe correlations. Our data are consistent with the stripe model where the charge domain is of length $\ell=6$ spins, and the domain correlations fall off over a length of 7 spins (~ 27 Å) as shown in Fig. 6. This fit was conducted by convolving the stripe model with the \mathbf{Q} resolution only and taking the energy dependence to have a simple Lorentzian form. One of the predictions of a sharp domain boundary is the presence of higher-order

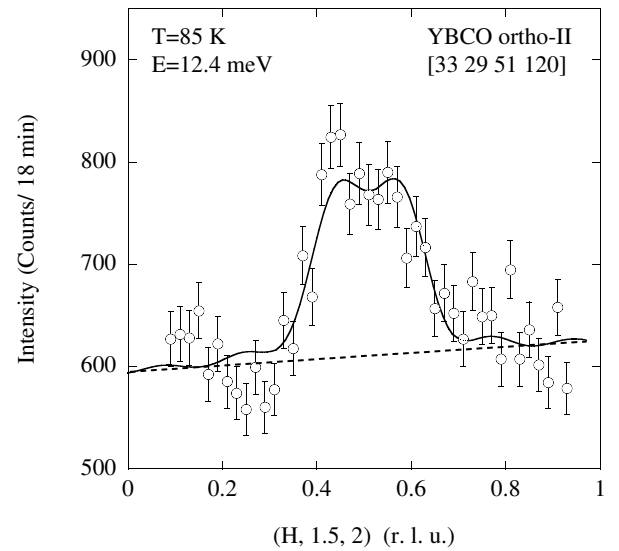


FIG. 6: The agreement of the stripe model (lines), in which antiphase domains of length $\ell=6$ with $\delta = 1/2\ell = 0.08$ occur with a correlation length of 27 Å, with the observed scattering near the antiferromagnetic wave vector $(1/2 \ 3/2 \ 2)$.

satellite peaks which are clearly washed out by the resolution. This model gives a δ of 0.08, slightly higher than that deduced using the Chou model but consistent given the errors of the fit and the fact that we have neglected energy dispersion in fitting the antiphase domain model.

Because our data are consistent with the idea that an incommensurate structure exists in the normal state, it is possible that the stripe phase is a precursor to superconductivity in the underdoped $\text{YBCO}_{6.5}$ system. The one-dimensional nature of the scattering is difficult to interpret as originating from band structure effects, for the small 1% a-b splitting should produce little difference in the bands and peaks in χ'' along the a^* and b^* directions. This is confirmed by density-functional calculations for the orthorhombic unit cell which predict nearly isotropic hopping integrals in the bandstructure.⁴² It seems more likely that the intrinsic structure of the spins (and carriers) in a plane favors stripe order and that the small a-b splitting as well as the filled oxygen chains serves to select a^* to orient the preexisting stripes.⁴³ Our results are similar to those found in the LSCO system. In particular, the incommensurate wave vector in this experiment is consistent with those found in the monolayer cuprates with the same hole doping.⁴⁴

A comparison of the incommensurability with doping for bilayer and single layer systems is shown in Fig. 7. As can be seen, our data are consistent with values of \mathbf{q}_{inc} observed in the LSCO system for similar hole doping. Even though data in the YBCO system are currently very limited, the good agreement to-date in the underdoped region points to a possible universal trend between the hole doping and the spin stripe width. Following Yamada *et al.*⁴⁴, Balatsky and Bourges⁴⁵ showed that the

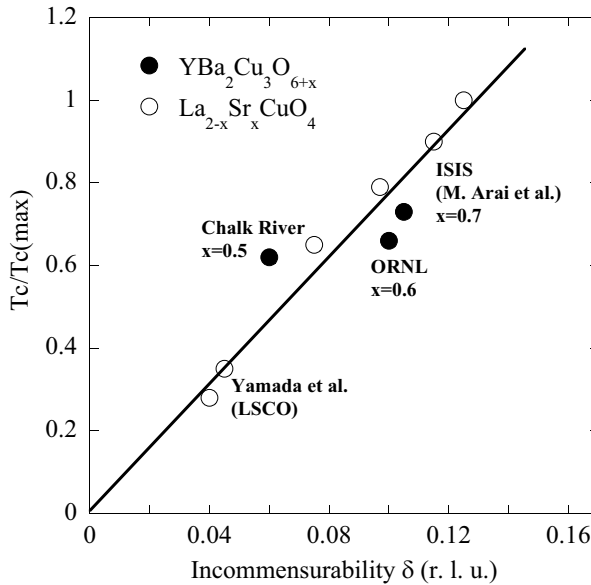


FIG. 7: The reduction of the superconducting transition temperature upon reducing the oxygen doping below optimum, as it relates to the position of the incommensurate peak in cuprate superconductors. The incommensurate wave vector along the Cu-O-Cu direction in reciprocal lattice units (r.l.u.) such that the wave vector is $2\pi\delta/a$.

overall half-width at half maximum of the Q-correlated peak below the resonance, whether it shows incommensurate modulation or not, is proportional to T_c . Our results are in agreement with this relation. This suggests that the widths in YBCO in part arise from incommensurate modulations and so can be interpreted within a stripe picture similar to that in LSCO.

The fact that δ is small, combined with short correlation lengths and twinning, could explain why many studies in this doping region have observed only a single commensurate peak at (π, π) . This point was the main assumption of the analysis of Chou *et al.* who fit a series of commensurate inelastic magnetic peaks to a model with spin waves originating, with equal weight, from the two slightly incommensurate positions of $\mathbf{q}=(0, \delta, 0)$ and $\mathbf{q}=(\delta, 0, 0)$.³⁴ It is also clear from our data that in a sample with equally populated structural domains, a single commensurate peak would be observed because of the small incommensurability.

The incommensurate correlations along a^* are a robust feature of the behavior and not a result of superconducting order in underdoped YBCO. They are present in the normal phase up to temperatures of at least ~ 120 K, and, as we shall see later, they persist in the superconducting phase up to ~ 25 meV (Fig. 13).

In scanning tunnelling microscopy Davis and collaborators⁴⁶ have observed a charge modulation along the b^* (chain) direction in optimally doped YBCO with a 13 Å periodicity cell. This would correspond to a reciprocal lattice wave vector of 0.3 r.l.u. In underdoped

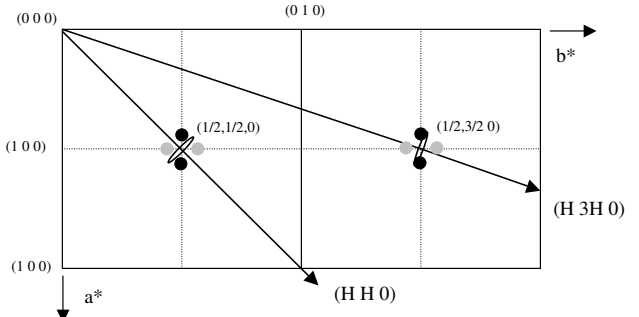


FIG. 8: Illustration of in-plane wave vectors accessible in the scattering planes (H 3H L) and (H H L). The actual scans were chosen to lie in the (H 3H L) plane so that the vertical resolution (ellipse) would integrate over the stronger incommensurate peaks along a^* .

YBCO_{6.5} there is no evidence for this modulation along b^* nor of any double-length spin modulation 0.15 r.l.u., both of which would have been easy to resolve. The spin modulation wave vector lies along a^* .

C. Temperature dependence of $\chi''(\mathbf{Q}, \omega)$ and ω/T Scaling in the Normal State

To study the Q-correlated peak as a function of energy and temperature, the sample was aligned in the (H 3H L) and the (H H L) scattering planes. This configuration was chosen so that the vertical resolution integrated over the intensity from the two slightly out-of-plane incommensurate peaks (see Fig. 8). Since the width of the Q-correlated peaks was found, within experimental resolution, to be independent of temperature, the peak susceptibility was then a good measure of the integrated intensity. To extract the susceptibility in absolute units we have removed the anisotropic Cu²⁺ form factor multiplied by the bilayer structure factor as discussed in the Appendices. The bilayer structure factor for odd-symmetry fluctuations will be shown later to give a good account of the L-dependence of the scattering.

The temperature dependence of the susceptibility is shown in Fig. 9 for energies of 12.4 meV and 24.8 meV. One of the most striking features is the presence of a clear suppression of the spin fluctuations at 12.4 meV below the superconducting transition temperature, as will be discussed in the next section devoted to the superconducting state. In the normal state, χ'' increases with decreasing temperature. As previously discussed this is further evidence for the absence of a normal state pseudogap in this energy range.

In early studies of the temperature dependence, χ'' in disordered YBCO_{6.5} was found to follow a simple ω/T scaling relation. The same ω/T scaling was very successful in describing the temperature dependence of the integrated susceptibility in underdoped La_{2-x}Sr_xCuO₄.^{47,48}

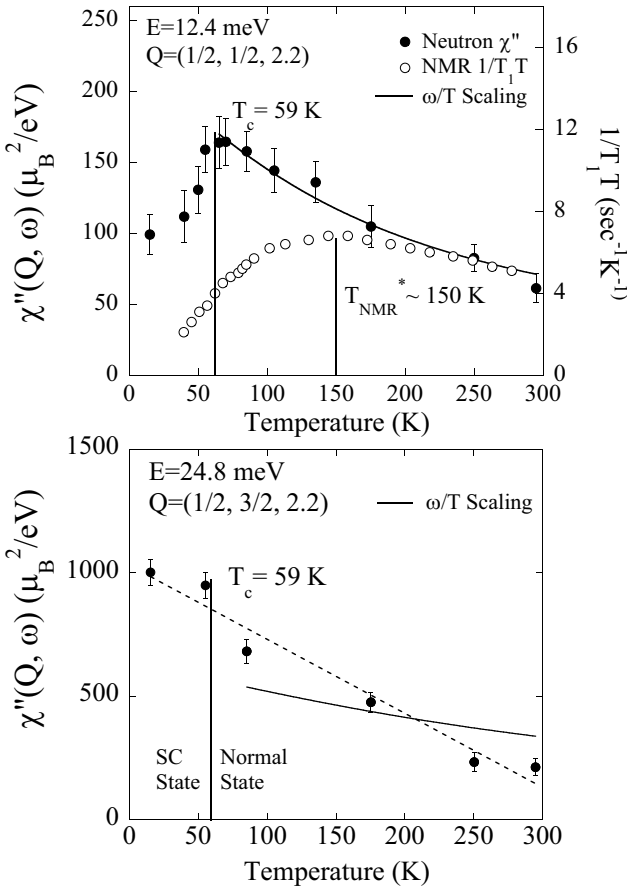


FIG. 9: The peak susceptibility at 12.4 meV and 24.8 meV as a function of temperature. For the normal phase, the solid curves are fits to the ω/T scaling analysis of Birgeneau *et al.* At 12.4 meV the normal state follows the scaling analysis. A clear suppression of scattering is observed in the superconducting state. The scattering at 24.8 meV in both the normal and superconducting states continues to grow on cooling and no longer follows the nearly constant temperature dependence predicted by ω/T scaling. The dashed line in the lower panel is just a guide. The local and low-frequency susceptibility sensed by the NMR relaxation rate of ^{63}Cu is suppressed on cooling below a temperature T^* , while the susceptibility at the antiferromagnetic wave vector increases uniformly until the onset of coherent superconductivity. NMR data is for $\text{YBCO}_{6.64}$ taken from Timusk and Statt.

The analysis assumes that the dominant energy scale is set by the temperature and predicts the following temperature and energy dependence of the scattering,

$$\frac{\chi''(\omega, T)}{\chi''(\omega, T = 0)} = \frac{2}{\pi} \arctan \left(\frac{\omega}{a_1 T} + \frac{\omega^3}{a_2 T^3} + \dots \right). \quad (5)$$

Here the term $\chi''(\omega, T = 0)$ represents the limit of χ'' as the temperature goes to zero. A detailed study on disordered $\text{YBCO}_{6.5}$ showed³⁶ that the temperature dependence of all scattering up to ~ 33 meV is described well by just the first term with a_1 set to 0.9:

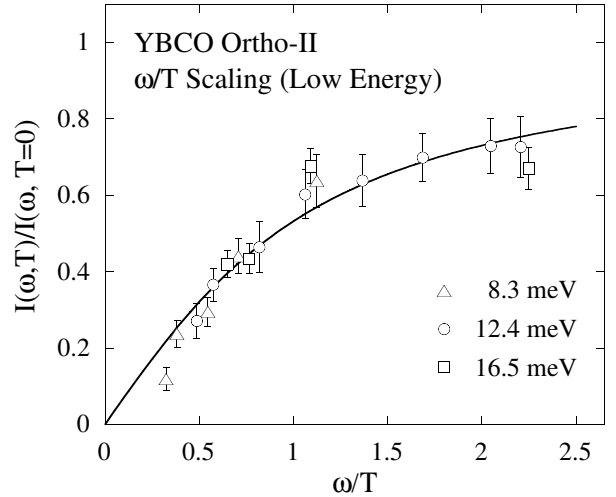


FIG. 10: A summary of the χ'' is plotted for all normal state data below 16 meV energy transfer as a function of ω/T . The temperature dependence of the low energy scattering is very well described by ω/T scaling.

$$\frac{\chi''(\omega, T)}{\chi''(\omega, T = 0)} = \frac{2}{\pi} \arctan \left(\frac{\omega}{0.9T} \right). \quad (6)$$

The inclusion of higher terms in the expansion was found not to noticeably improve the fits. This scaling was also originally proposed in the context of the marginal Fermi liquid theory to explain many of the normal state physical properties of the cuprates.⁴⁹

For ordered $\text{YBCO}_{6.5}$ in its ortho-II state we find that in the normal phase this scaling form is in excellent accord with the spin response at low-energies. Surprisingly the scaling function fits the data with the *same* coefficient $a_1=0.9$ as for the disordered system. The relation is plotted in the normal state for 12.4 meV and 24.8 meV transfers in Fig. 9 and shows excellent agreement at 12.4 meV but not at 24.8 meV. The results for energy transfers below 20 meV are summarized in Fig. 10. The figure was obtained by fitting (with $a_1=0.9$) the ω/T scaling relation at each energy to derive a single parameter $\chi''(\omega, T = 0)$, from which $\chi''(\omega, T)/\chi''(\omega, T = 0)$ follows for all temperatures and energies. We conclude that ω/T scaling accurately describes the normal state low-energy $\hbar\omega$ and temperature dependence.

Despite the fact that the scaling analysis works very well for low energies, the scaling previously observed and predicted suggests that for higher energy transfers the integrated susceptibility should be only weakly dependent on temperature. This is clearly not the case at 24.8 meV (Fig. 9) where the response grows strongly on cooling. It also does not hold at higher energies where we see χ'' increasing continuously with decreasing temperature. This difference in scaling in the normal state shows a clear departure of the scattering in YBCO ortho-II from that in the disordered systems previously studied which ob-

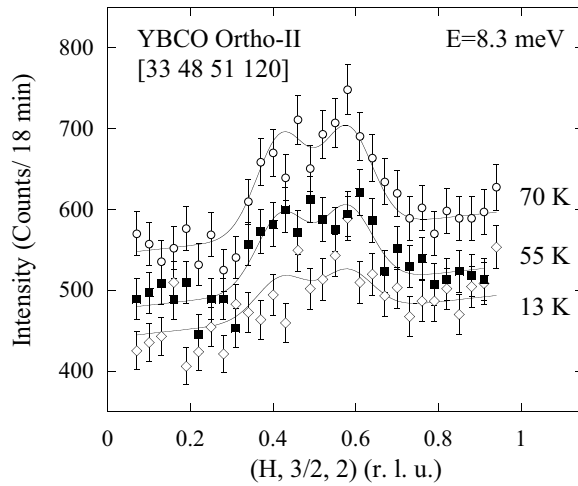


FIG. 11: Constant energy scans of the scattering at 8.3 meV energy transfer. The incommensurate behavior persists unchanged apart from amplitude upon entering the superconducting state. The background beyond the peaks and the fast neutron background scales as $[n(\omega)+1]$. The solid lines are from double Gaussian fits to the data.

served scaling up to at least 33 meV. We note that a breakdown of ω/T scaling has been observed at very low energies in $\text{La}_{1.98}\text{Sr}_{0.02}\text{CuO}_4$ and is thought to originate from a small gap in the excitations due to the out-of-plane anisotropy.⁵¹

A possible explanation for the presence of one-dimensional incommensurate scattering, ω/T scaling, and the breakdown of the scaling relation at higher energies can be found in the stripe model. The stripes consist of one-dimensional domains π out of phase with each other. As discussed by Zaanen *et al.*⁵⁰ for a stripe liquid, where there is no long-range order and stripes are fluctuating, there are two extreme energy scales. The first is at high energy where the domain walls appear static, and the second is the hydrodynamic limit where the stripes are in a fluid state. For the second hydrodynamic (low energy) limit the energy scale of the system is set by the temperature. These assumptions underlying ω/T scaling suggest that the fluctuating stripe model provides a natural explanation for the ω/T scaling we clearly observe at low energies in the normal state. It is also argued by Zaanen *et al.* based on hydrodynamics that $\chi'' \sim \omega/T$ which can also be derived from the ω/T scaling relation by expanding the expression to first order. Therefore stripes do not predict the presence of a spin pseudogap in the normal state but predict scattering at all energies and that $\chi'' \sim \omega$ at low energies. This is exactly the model applied here to our low scattering and originally used by Chou *et al.* This is further illustrated in Fig. 4 which shows the scattering at very low energies decreasing as ω .

The stripe model also predicts the breakdown of ω/T scaling. At some point the energy will be sufficiently

large compared with the fluctuation frequencies that the fluid domains will appear almost static. In our lineshape analysis this energy would be given by $\omega_c \sim \hbar c/\xi_0 = 300 \text{ meV} \cdot \text{\AA}/20 \text{ \AA} = 15 \text{ meV}$. Therefore we would expect that for energies above $\sim 15 \text{ meV}$ the internal domain dynamics will start to play a role in setting the energy scale and lead to a breakdown of ω/T scaling. This is qualitatively what is seen in our data - perfect ω/T scaling up to at least 16 meV followed by a clear departure from scaling at 25 meV.

These qualitative ideas can be extended to explain the role of disorder. Disorder would decrease the correlation length ξ and therefore increase the characteristic frequency ω_c . This would provide a natural explanation for why early studies on highly disordered crystals followed scaling up to high energies $\sim 33 \text{ meV}$. These arguments provide some support to the idea that the presence of fluctuating stripes in a liquid phase can explain many qualitative features of the data in the normal state including the temperature dependence and lineshape.

ω/T scaling can also be interpreted as the result of the close proximity of a quantum critical point where energy and temperature are interchangeable. Such critical points have been suggested to exist in the over-doped and near optimally doped region of the generic cuprate phase diagram.^{52,53} The fact that we observe scaling in the underdoped region and that scaling is observed over a broad region in the LSCO system suggests that the scaling is not the result of a quantum critical point. This assertion does depend on the extent and size of the cross-over region. To address the issue of quantum criticality clearly a more detailed study as a function of hole doping would be required in the YBCO_{6+x} system.

IV. SUPERCONDUCTING STATE

A. Suppression of Low Energy ($\leq 16 \text{ meV}$) Scattering

On entering the superconducting state, the scattering at energies less than $\sim 16 \text{ meV}$ is suppressed but not eliminated as shown in Figs. 4, 9, 11 and 12. Thus there is not a complete gap. Moreover, the incommensurate structure remains in the superconducting state. As shown in Fig. 9 the suppression clearly starts at T_c and cannot be taken as evidence for a normal phase pseudogap as previously discussed. This suppression at the onset of superconductivity clearly departs from the ω/T scaling relation, in contrast to what was derived from early studies on disordered systems for similar oxygen concentrations. Our measurements also agree qualitatively with the result of early studies on higher oxygen dopings which showed a departure from ω/T scaling and a suppression of scattering in the superconducting state.⁵⁴ This response is consistent with the behavior in underdoped LSCO, where the low energy scattering has been found to be suppressed in the superconducting state⁵⁵ with almost complete gap-

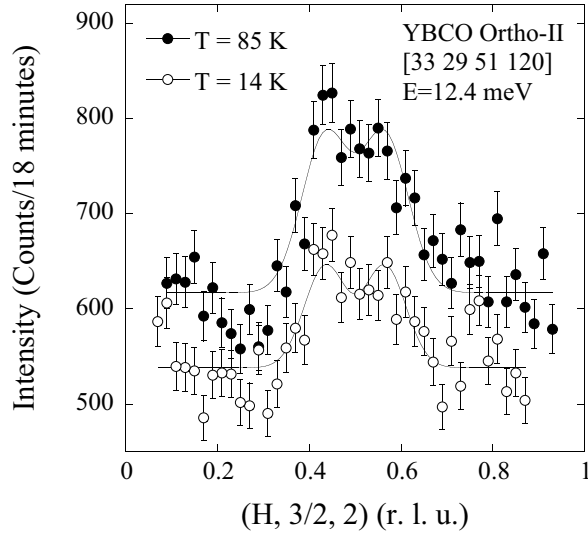


FIG. 12: Constant energy scans of the scattering at 12.4 meV energy transfer. The lineshape does not change upon entering in the superconducting state. The background scales as $[n(\omega) + 1]$. The solid lines are from double Gaussian fits to the data.

ping at the lowest energy.⁵⁶ For YBCO_{6.5} we find that the energy below which the response is suppressed in the superconducting state is consistent with the *gap* derived by other groups in the YBCO_{6+x} system for higher doping.⁵⁷

Thus, although there is no evidence for a normal phase gap, there is clear evidence of formation of a gap as superconducting order develops, with the degree of gapping increasing as the energy tends to zero as seen in Fig. 4. We do not observe a full gap, and indeed would not expect to do so in a superconductor where the pairing gap has nodes, regardless of the gap symmetry.

In contrast to the suppression of the superconducting response below ~ 16 meV, for energies greater than 24 meV the response is enhanced (Fig. 9). It is interesting to compare this observation to simple BCS theory which predicts a gap at $2\Delta = 3.5k_B T_c \sim 18$ meV. The temperature dependence of χ'' for both the s-wave and d-wave cases have been computed in the random-phase approximation by Bulut and Scalapino.⁵⁸ Their calculation was done assuming a single band with only nearest neighbor hopping. The hole doping was $p=0.15$, somewhat above the doping of $p=0.09$ that is estimated for our ortho-II YBCO system from its T_c . For a gap with s-wave symmetry the imaginary part of the susceptibility shows a strong suppression or gap at all energies up to the $\hbar\omega \sim 2k_B T_c$. The d-wave model shows a suppression for energies below $\hbar\omega \sim k_B T_c$ and an enhancement for energies of $k_B T_c$ and above. The d-wave results capture only the qualitative trend of our data, in the sense that they show suppression at low energies and enhancement at high energies. Quantitatively, however, the model fails to predict

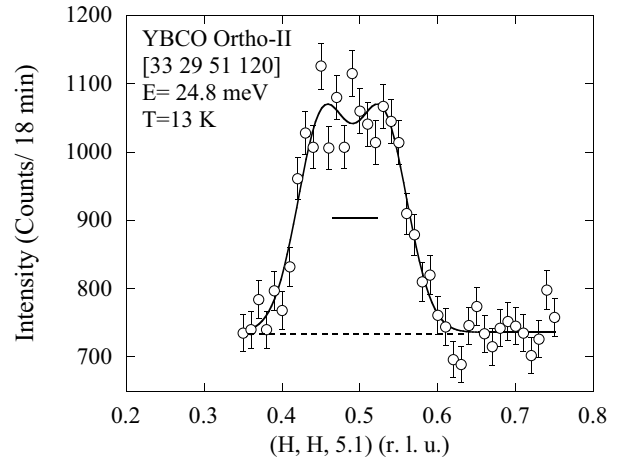


FIG. 13: Constant energy scans of the scattering at 24.8 meV energy transfer showing a clear flat-top lineshape indicative of incommensurate scattering. This scan was performed in the (HHL) scattering plane. The solid line is from a double Gaussian fit to the data.

the energy scale at which the crossover from suppression to enhancement occurs, for it predicts $E \sim k_B T_c$, which is ~ 5 meV, whereas we observe crossover at ~ 16 meV or $\sim 3k_B T_c$. Despite this disagreement the general trend of our data is consistent with the formation of a d-wave instead of an s-wave gap which would show a suppression of the scattering at all energy transfers.

As regards the spatial spin correlations we observe that they continue to exist with the same incommensurate form in the superconducting phase as they did in the normal phase, and this despite the suppression of the susceptibility by the superconducting order. The dynamic stripe structure is robust not only with respect to temperature, but also with respect to energy, for it is present up to ~ 25 meV as illustrated in Fig. 13.

In the context of the stripe picture previously discussed for the normal phase, we observe that the spin suppression in the superconducting phase occurs over an energy range similar to that of the hydrodynamic region of the striped normal phase, i.e., the energy range where we found that ω/T scaling describes the normal state temperature dependence. This suggests that the superconducting order acts to suppress the amplitude of the precursor stripe fluctuations of the normal phase, but does not essentially change their spatial or temporal character.

B. Resonance at 33 meV

One of the most dominant features of the scattering in the superconducting state, as shown in Fig. 14, is the presence of an intense and well-defined peak in energy at 33 meV energy transfer. We have verified that this resonance peak is magnetic in origin from three features: it exhibits the clear L dependence (Fig. 15) expected

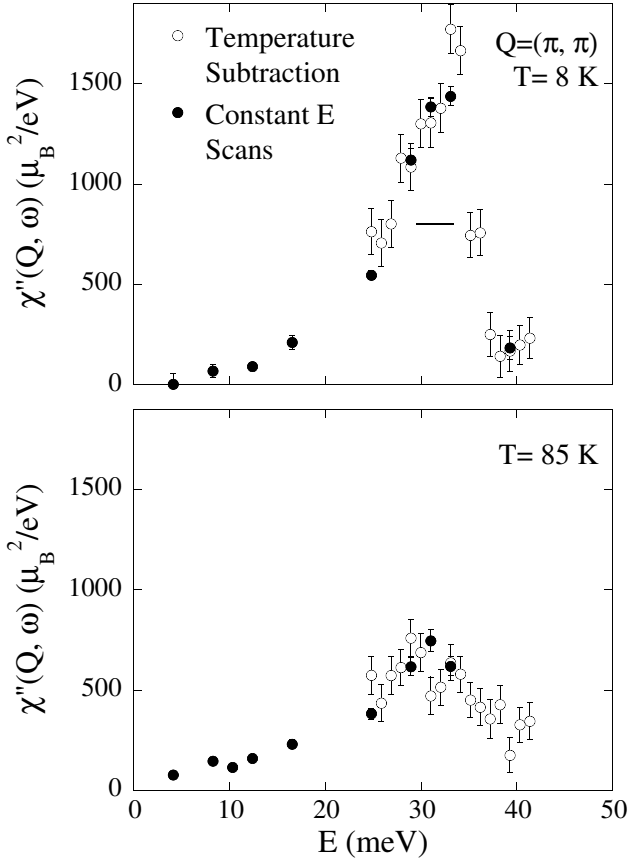


FIG. 14: χ'' for all energies studied is summarized in both the normal and superconducting states. Two methods of measuring χ'' are plotted, the solid points being obtained from constant-energy scans and the open points from a direct subtraction of the high-temperature background measured at 250 K. A clear resonance appears in the superconducting state and also in the data at 85 K, indicating that a resonant feature does persist into the normal state.

for the bilayer structure factor of the two copper oxide planes, its intensity decreases with increasing temperature as does magnetic scattering (Fig. 18), and it appears in polarized neutrons in the purely magnetic difference channel, as will be discussed later.

In Fig. 15 we show that the bilayer structure factor, scaled by a single amplitude, gives an excellent account of the modulation of the resonance intensity along the [001] direction. The scan in Fig. 15 was done by conducting a series of one-point scans on and off the peak and subtracting. The fact that the data are negative at the minimum of the bilayer indicates the presence of a sloping background. We have also verified that the scattering follows the anisotropic Cu^{2+} form factor by comparing constant energy scans done at the $(1/2, 1/2, 2)$ position to equivalent scans conducted at higher $|\mathbf{Q}|$ Brillouin zones. This shows that the resonance is consistent with scattering from Cu^{2+} spins in the planes which fluctuate in antiphase between the bilayers (also known

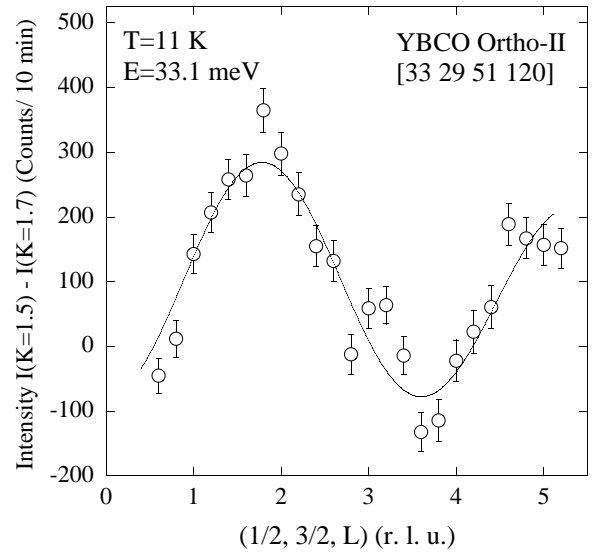


FIG. 15: Constant energy scan through the resonance along the [001] direction. Due to the presence of optic phonons a series of two point scans were done with data being taken on and off the peak. The solid line is a fit to the bilayer structure factor. The fact that the subtraction gives negative values at the minimum of the bilayer structure factor indicates the presence of a sloping background.

as the acoustic or odd-symmetry mode).

We find, as have others,²⁹ that the resonance is commensurate. Scans along $(\text{K}/3, \text{K}, 2)$, $(\text{H}, \text{H}/3, 2)$, and $(\text{H}, \text{H}, 5)$ directions geometries have been used in previous studies to investigate the incommensurate scattering as a function of energy and temperature.⁵⁹ We have determined that the resonance is commensurate by scanning along along the $(\text{K}/3, \text{K}, 2)$, $(\text{H}, \text{H}/3, 2)$, and $(\text{H}, \text{H}, 5)$ directions. The latter two scans are sensitive to any incommensurability in \mathbf{Q} along a^* and showed incommensurate peaks for energies below 24 meV. However at the resonance we observe only a single commensurate peak, an example of which we display in Fig. 16. Its width (FWHM) in \mathbf{Q} , after correcting for resolution, is $\sim 0.17 \text{ \AA}^{-1}$, implying a correlation length of 12 \AA or about 3 cells.

In the ortho-II ordered sample the susceptibility shows a linear region followed by a clear upward curvature to a well-defined resonance at 33 meV (Fig. 14) with a half-width of 3.6 meV (including resolution). In contrast, when the system has the same $x=0.5$ oxygen content, but is disordered, the linear region of the local susceptibility leads to a broad maximum at ~ 15 meV without the upward curvature typical of a resonant mode.⁶⁰ This broad feature, with a half-width of ~ 14 meV, extends to low energies and differs substantially from the spectral form for the well-defined resonance of the well-ordered the ortho-II system. In another $x=0.5$ sample with $T_c=52$ K the peak of the resonance occurred at \sim

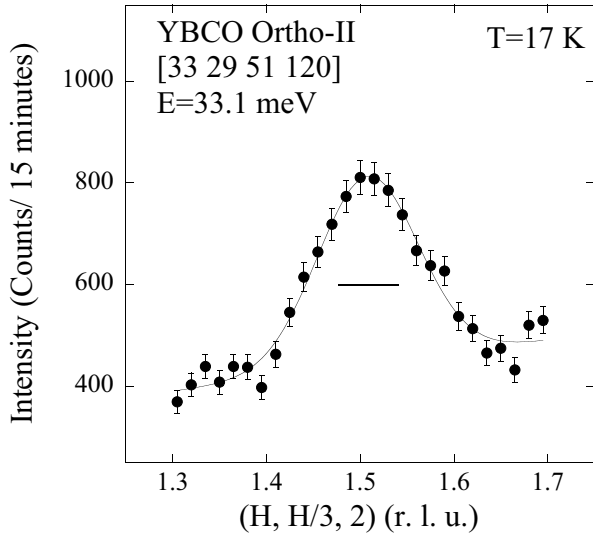


FIG. 16: Scan through the 33 meV resonance at $(3/2\ 1/2\ 2)$, a direction that is sensitive to any incommensurate modulation along a^* such as was observed well below the resonance. A single commensurate resonance peak is observed whose width exceeds the resolution (horizontal bar).

25 meV again without upward curvature.⁶¹ The large differences suggests that the effect of structural disorder in the chains is to damp out the resonance. Indeed the resonance is broadened in disordered systems to give a tail on its high-energy wing, resulting in a more symmetric resonance, whereas in ordered ortho-II we find a sharp resolution-limited decrease above the resonance. When the disorder is small, as in the present ortho-II crystal, the resonance becomes quite long-lived (of order 10 periods from the raw data and longer if resolution is allowed for). Also, this naturally explains why in early studies the resonance was first discovered in optimally doped systems. These have all the chains nearly full and so no oxygen disorder is present (i.e., ortho-I chain ordering), while for lower doping without stress detwinning a much broader version of the resonance is seen.^{60,61} As far as the effect of disorder on the width in \mathbf{Q} , we can understand why, in the comprehensive study of Dai *et al.*²⁹, the sample with the most developed oxygen order, YBCO_{6.6}, as determined from clear ortho-II oxygen peaks, exhibited a much sharper resonance in \mathbf{Q} than did other samples.

This line of thought would suggest that the resonance should be strongly broadened in the LSCO system because Sr enters the lattice in a disordered manner, therefore having the analogous effect to disordered oxygen chains in YBCO. To-date there has been no clear sign of a resonance in LSCO. However, there is evidence for doubling of the strength of the local susceptibility, relative to that in the antiferromagnetic insulator, at ~ 20 meV, just above the superconducting gap.⁶² This could be taken as evidence that the superconducting order pushes the spectral weight to a region above the gap.⁵⁶ If this feature was

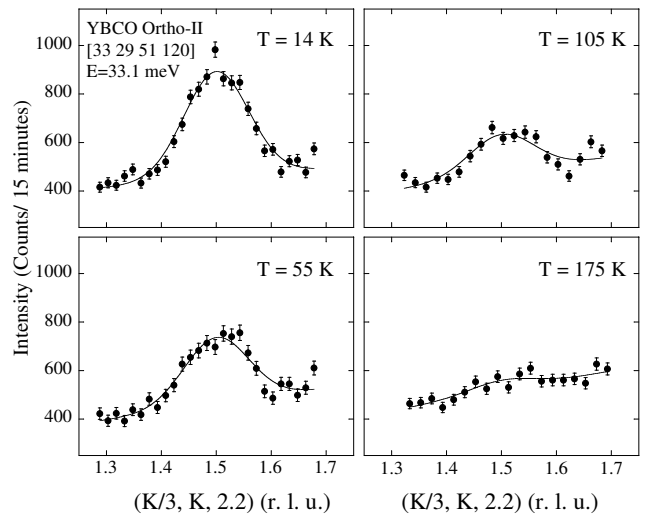


FIG. 17: Constant energy scans through the resonance peak as a function of temperature. The fits are to Gaussian peaks with the fixed width for all temperatures. A clear peak is seen in the superconducting state and it persists in the normal state until it almost unobservable at 175 K.

taken as the analog of the YBCO resonance, its spectral form is substantially different since it is broad with a tail to high energies, but may nonetheless be consistent with the effects of disorder. The resonance has been found in monolayer compounds indicating that a bilayer structure is not necessary for its presence.¹⁸

Fig. 17 shows constant energy scans at 33 meV for several temperatures. These scans show that the \mathbf{Q} correlations at the resonance energy still exist well into the normal state. Fig. 18 shows the growth upon cooling of the peak susceptibility at 33 and 31 meV. The spin response exhibits a very clear upward break in slope at the onset of superconductivity and is clearly enhanced below T_c . What is plotted is the peak in absolute units derived from the constant-energy scans of Fig. 17. A normal phase resonance at 34 meV was observed⁶³ below 150 K in YBCO_{6.6} and used to define a pseudogap temperature. The resonance energy was found to increase with temperature. The resonance intensity in ordered YBCO_{6.5} is still visible at 175 K, particularly if the scan follows the resonance energy down to 31 meV as it decreases on heating.

To establish that in the normal phase the 33 meV feature is resonant in time as well as localized in \mathbf{Q} it is important to observe that its width is less than its energy in a constant- \mathbf{Q} energy scan. To remove the effects of phonons we have subtracted a background scan taken at 250 K. Since the magnetic scattering, as determined from constant energy scans, at energies greater than ~ 24 meV, essentially disappears by 250 K this method of subtraction should give the full peak susceptibility $\chi''(\mathbf{Q}, \omega)$. We have also subtracted an estimate for the temperature independent background by rotating the analyzer crystal five degrees and counting. As can be seen from Fig. 19,

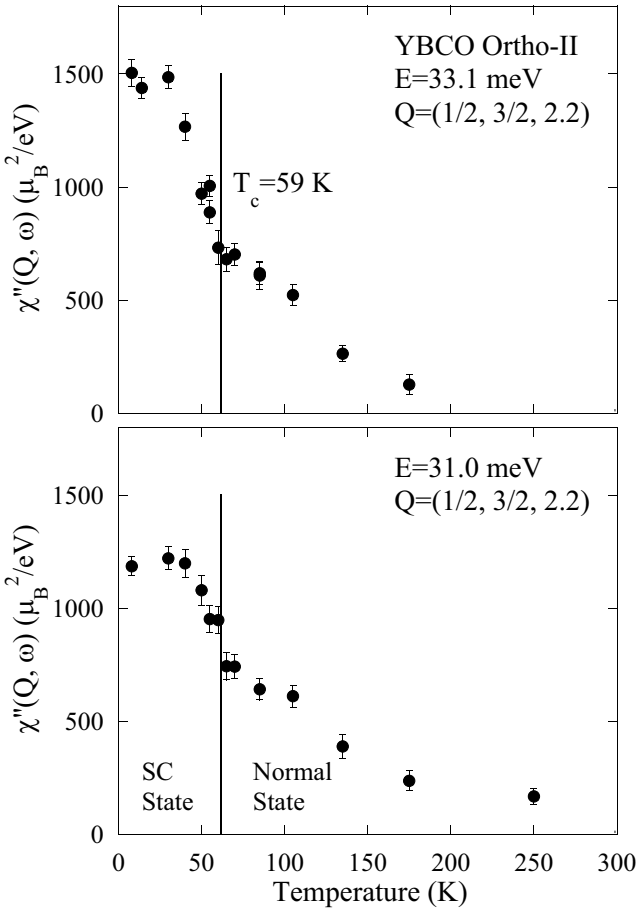


FIG. 18: The peak intensity as obtained from constant energy scans of the scattering at 33 and 31 meV is plotted as a function of temperature. Both sets of data show a clear enhancement of the intensity at T_c and presence of a resonance peak at $\mathbf{Q}=(\pi, \pi)$ well into the normal state.

where results for three of the temperatures studied are shown, the method of subtracting high-temperature data does a reasonable job at removing the phonons. There is a very intense optic phonon at 20 meV which does not quite subtract out and gives an apparent rise in scattering around this energy. Nevertheless the energy scans show the clear resonance below T_c and reveal that in the normal state the resonance remains as a weaker but still well-defined feature.

The lines in Fig. 19 are a fit to a Lorentzian and a temperature dependent background. We fixed the width at all temperatures to obtain a stable fit in the normal state. The quality of the data above T_c prevents us from determining whether or not the resonance broadens in the normal state. The fit, though, does suggest that the peak of the resonance shifts to higher energy (as shown in the inset to Fig. 19) with decreasing temperature, reminiscent of a slight decrease in damping with decreasing temperature. This shift in resonance frequency with decreasing temperature can be explained by the spin-fermion model

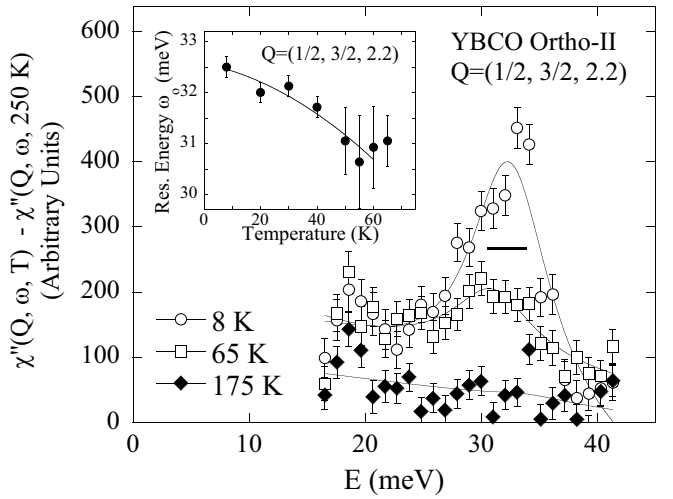


FIG. 19: Constant \mathbf{Q} scans obtained from a temperature subtraction with data at 250 K taken as the background and with the Bose factor removed. The rise around 20 meV is due to a strong optic phonon which does not completely subtract out in our analysis, giving a sloping background. The data shows a clear resonance in the superconducting state. The 65 K data indicate that a weakened resonance persists into the normal state. The lines are a Lorentzian on a sloping background. The inset shows that the resonance energy decreases slightly with increasing temperature.

of Morr and Pines.²⁰ In the spin-fermion model the resonance position is predicted to be inversely proportional to the magnetic correlation length. We should emphasize, however, that we do not explicitly measure any temperature dependence of the correlation length. A similar result has been obtained by Fong *et al.*⁶⁹ for optimally doped YBCO.

The energy integrated resonance intensity as a function of temperature from constant \mathbf{Q} scans is seen from Fig. 20 to show a clear enhancement below T_c . Two methods were applied to estimate the energy integral. In one (closed circles) we took the area under a fitted Lorentzian. The background fitted under the Lorentzian removes from the estimated area part of the response that grows on cooling in the range 25-33 meV (in Fig. 19 compare $T=65$ K with 175 K); it tends to underestimate the integral e.g., at 65 K, but is more accurate at low temperature where the resonance is strongly peaked. Furthermore we know from low temperature data that the resonance carries a long tail to low energies which is not accounted for by a symmetric Lorentzian fit. Since we know the range 25-33 meV to be free of phonons in our temperature-subtracted data (see polarized data later), we adopted a second method for the spectral weight in which we numerically summed the observed response from 25 to 43 meV (open circles in Fig. 20). This method will account, as we see, for less than the full integral at low temperatures.

The fraction of the full superconducting resonance in-

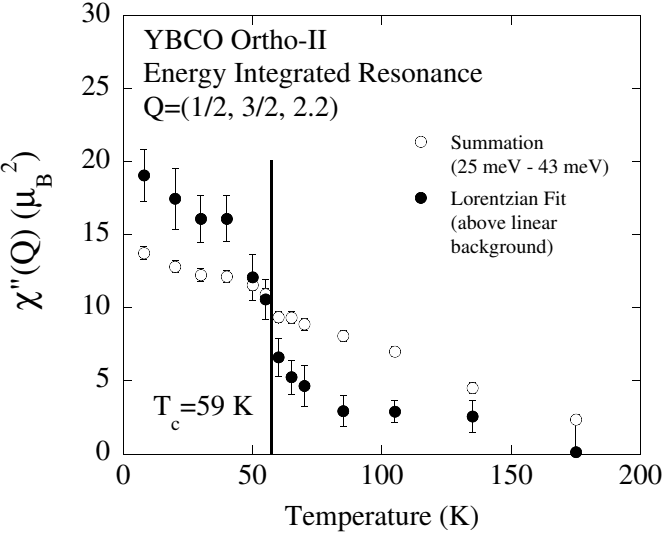


FIG. 20: The energy integrated intensity of the resonance as measured in constant \mathbf{Q} scans. The integrated intensity in absolute units was obtained by summing the data from 25 to 43 meV, and also by fitting a Lorentzian to data like Fig. 19. The latter method gives a resonance integral that reaches a maximum of $\sim 19 \mu_B^2$ at low temperature. There is a clear increase in the growth rate of the resonance intensity on entry to the superconducting state. Both methods show that a substantial fraction of resonant precursor is already present in the normal state.

tensity that remains in the normal phase just above T_c (Fig. 20) is 25% from the Lorentzian fits and 70% from the numerical integration. Either estimate is a substantial fraction of the low-T resonance, as we already found from the the peak height of the \mathbf{Q} -scans (Fig. 18) where 45% survives. We conclude that the resonant feature exists in the normal phase as a temporal and spatially correlated feature, indicative, as discussed later, that superconducting fluctuations persist in the normal phase. As a fingerprint for pairing it appears that of order half the superconducting density, albeit incoherent, has already formed in the normal phase.

By combining both methods, \mathbf{Q} -scans and constant \mathbf{Q} energy scans using temperature subtraction, we have been able to arrive at a complete picture of the magnetic spectrum up to 40 meV as shown in Fig. 14 in both the superconducting (8 K) and normal (85 K) states. The spectrum is obtained at high-resolution because we used a low final neutron energy of 14.4 meV for even the largest energy transfers. The absolute calibration was determined against the known cross-section of an acoustic phonon assuming a paramagnetic (isotropic in spin) cross-section (see Appendices). The two methods for determining $\chi''(\mathbf{Q}, \omega)$ agree very well, further indicating the validity of the assumptions used in the subtraction analysis previously discussed.

In Fig. 21 we plot the dependence of the low temperature resonance frequency on doping (derived⁷⁰ from T_c)

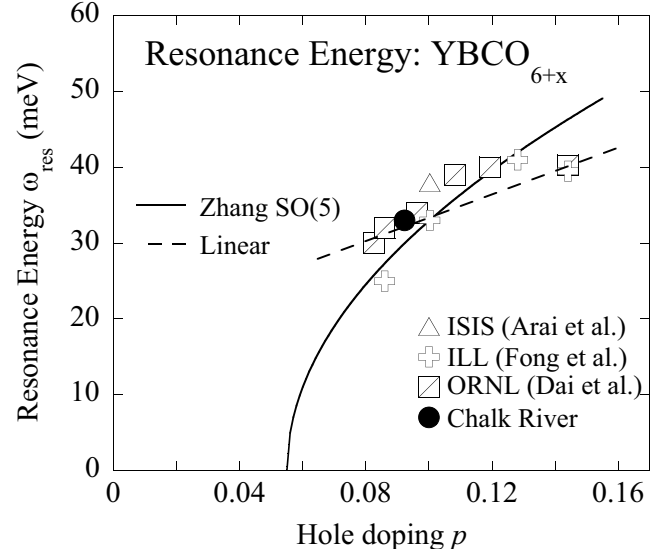


FIG. 21: A summary plot of the resonance energy as a function of hole doping p for the YBCO_{6+x} system. The solid line is a fit $\omega_{res} \propto (p-p_c)^{1/2}$ as predicted from SO(5) theory. The dashed line is a linear fit. Both fits give reasonable descriptions of the data.

as determined by different groups. It can be seen that the resonance frequency in our sample is consistent with the overall trend. A linear scaling of the resonance energy with T_c (dashed line) is consistent with most of the data. However the resonance trend also lies close to the predictions of the SO(5) model⁶⁴ for which the solid line is a fit to $\omega_{res} \propto (p-p_c)^{1/2}$ with $p_c=0.055$, as measured carefully in the LSCO system⁶⁵. Because its spectral weight has a strong onset at T_c for optimally doped, and an accelerated growth rate at T_c for underdoped, there is little doubt that the resonance peak is intimately related to superconductivity. It is not yet clear which effect drives the other; the pairing could involve the entire very high energy spin-wave band while the resonance is a consequent low-energy concentration of spin response caused by the pairing. Further studies, particularly at lower doping, are required to address this point. We will discuss this topic later in the context of the total integrated intensity and the sum rule.

At low temperatures we clearly see the presence of both a commensurate resonance peak, and incommensurate scattering at low energy transfers. This coexistence points to a possible common origin of both the resonance and incommensurate scattering. This topic has been discussed by Batista *et al.* who have analyzed possible common magnetic origins of both the resonance and incommensurate scattering.^{66,67} In the analysis of Batista *et al.* the incommensurate features are interpreted as spin-waves originating from incommensurate wave vectors. A resonance then results when the spin-wave branches meet at the (π, π) position. This idea connects with our data as our line shape found in the unpolarized data has a

clear tail at low energies and is suggestive of an umbrella type dispersion where the excitations meet at the resonance position. Such a dispersion in the context of the incommensurate to commensurate behavior has been discussed in studies of optimally doped YBCO.⁵⁹ However, these ideas are speculative for YBCO_{6+x} as the incommensurate scattering is broad and we cannot resolve the spin-wave branches suggested by this analysis.

It is not clear how the low-energy fluctuating stripes relate to the resonance peak. In the normal state we see formation of incommensurate fluctuations below ~ 120 K or $2T_c$, comparable but a bit lower than the temperature ~ 170 K or $3T_c$ below which the resonance first becomes observable. On cooling the resonance grows faster than the incommensurate stripe response, whose susceptibility increases down to T_c before declining. The growth of resonance intensity accelerates on passing into the superconducting phase, concomitant with the onset of suppression of the stripe fluctuations. Whether one or the other is the progenitor remains an open issue.

C. Polarization Analysis

To determine if there is any preferred orientation for the spin fluctuations we studied the resonance and low-energy scattering in three different zones and scattering planes. These included the (H, H, L), (H, 3H, L), and (3K, K, L) zones. With unpolarized neutrons the low-energy incommensurate scattering and the resonance peak do not show measurable asymmetry between the (H, 3H, L) and (3H, H, L) directions. This rules out any enhanced spin fluctuations oriented along either the a^* or b^* directions. A comparison of the intensity in the (H, H, L) plane with that in other scattering planes suggests no preferred spin fluctuations along the c^* direction. This is the same isotropic spin polarization behavior as in a paramagnetic phase.

Further evidence for this finding comes from polarization analysis. For scattering from a paramagnetic material with a horizontal field (HF) along \mathbf{Q} , all of the magnetic scattering will appear in the spin flip channel since the neutron detects only the perpendicular component of the magnetization. For a vertical field (VF) perpendicular to \mathbf{Q} the magnetic scattering will contribute equally to the spin-flip and non-spin-flip channels. If the magnetic scattering is entirely paramagnetic, the scattering in the HF channel will then be exactly twice that in the VF channel. Fig. 22 shows polarized scans through the resonance at three different temperatures. The HF intensity is always twice that in the VF channel to within error, showing that the scattering arises only from the magnetic spins and that the resonance is isotropically polarized. The fact that we see no preferred polarization in the spin fluctuations is consistent with transitions from a singlet superconducting ground state to a triplet excited state. We note that a triplet particle-particle resonance, coupled by the superconducting order parameter into the

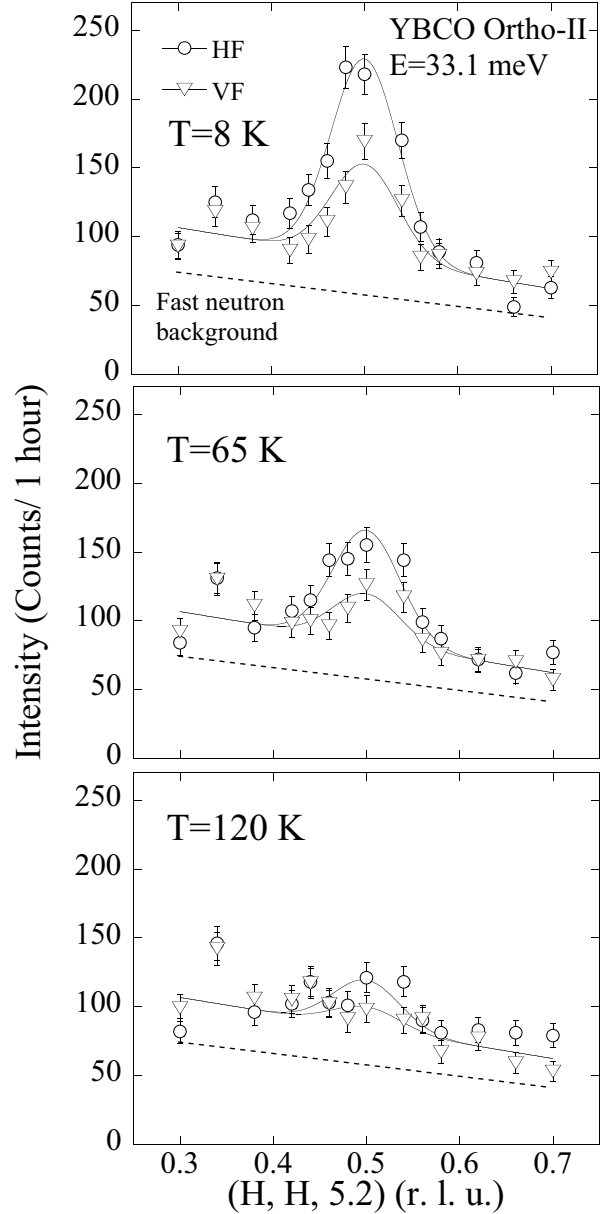


FIG. 22: Polarized constant energy scans through the resonance peak at temperatures below and above T_c . The decrease with temperature of the resonance intensity at 8 K agrees with that of the unpolarized data, eliminating any possibility of phonon contamination. The open circles are taken with guide field parallel to \mathbf{Q} (HF) and the triangles with field perpendicular to \mathbf{Q} (VF). The peak intensity in the VF channel is roughly half that in the HF channel, which indicates no preferred polarization of this excitation. The dotted line is an estimate of the fast neutron background. The feed-through from the NSF channel can be estimated from the flipping ratio to be on average ~ 10 counts. When added to the fast neutron background, this almost completely accounts for the background around the correlated peak. The temperature dependent high point at $H=0.35$ also appears in the NSF channel and is likely due to a phonon. The solid lines describe Gaussian fits to the data.

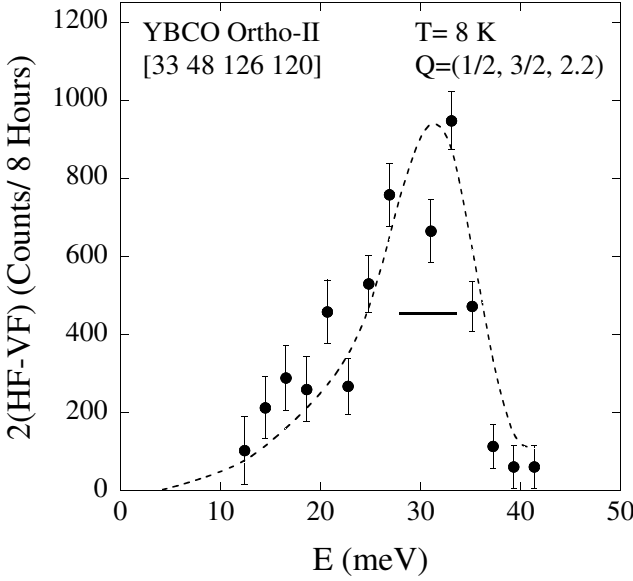


FIG. 23: Polarized measurement of the spectral form of resonance peak obtained by subtracting the vertical field (VF) from the horizontal field (HF) data. The 33 meV peak position, the resolution limited high-energy cut off, and the low-energy tail connecting to the incommensurate response, confirm the spectral form got from the unpolarized data (dotted line is smoothed unpolarized data scaled by a constant factor).

particle-hole spin susceptibility, is predicted by the SO(5) theory of Demler and Zhang⁶⁸.

The temperature dependence of the resonance intensity agrees with that obtained from the unpolarized constant energy scans. The agreement proves that magnetic resonance scattering persists in the normal state at 65 K. Since the scattering disappears at high temperatures, this unambiguously demonstrates the absence of any contamination from accidental Bragg or phonon scattering. This type of contamination has been a problem in previous studies of the resonance mode.^{16,69}

Fig. 22 also shows that the background around the resonance peak has the same intensity in the HF and VF channels. This indicates that there is no measurable continuum or diffuse magnetic scattering other than the antiferromagnetic correlations centered on the (π, π) position. This point is further highlighted by the dotted line in Fig. 22 which gives the fast neutron count with the analyzer rotated five degrees. Even though this method does not obtain the full background, it does put a lower bound on the amount of background scattering. From this one can see that most of the background is taken into account by the scattering with the analyzer turned. The rest of the spin-flip intensity in the wings is close to that expected from feed-through from the non spin-flip channel. This contribution to the scattering in the spin-flip channel is equal to the scattering in the non-spin-flip (NSF) channel divided by the flipping ratio. This is equal

to approximately 10 counts for the monitor used in Fig. 22. The NSF feed-through and fast neutron rate account for almost the entire background. This shows that there is no measurable magnetic diffuse or continuum scattering around the correlated peak at (π, π) . Finally, we note that in this energy range there is no observable scattering from hydrogen. This would have occurred as nuclear spin-flip scattering equally in VF and HF channels. This attests to the careful mounting of the sample in dry conditions²⁵ and to the minimal amount of shielded adhesive used to seal the sample cans.

Since it is established that the scattering is paramagnetic, we have been able to independently verify that the low temperature spectral line shape derived from unpolarized data (Fig. 14 is correct. We subtracted the spin-flip scattering at $(1/2, 3/2, 2.2)$ in HF and VF channels and so obtained the magnetic scattering alone, free from the phonon contamination which we had to remove in analyzing the unpolarized data. The resulting spectral form of the resonance shown in Fig. 23 is in excellent agreement with the unpolarized results (the dotted line shows the smoothed unpolarized data). In particular, the polarized scans confirm the interesting asymmetric line shape consisting of a low-energy tail leading to a sharp cut-off beyond the peak of the resonance as discussed above.

D. Integral of $S(Q, \omega)$ and the Sum Rule

From Fig. 14, we have estimated the total integrated spectral weight of the resonance at 8 K. To do this a symmetric Lorentzian profile centered at 33 meV was fit to the low temperature energy scan in Fig. 14 to obtain a half-width $\Gamma=3.6$ meV and a peak intensity of 1400 μ_B^2/eV . By assuming a Gaussian line shape along both the [100] and [010] directions, a perfect column of scattering along the [001] direction, and ignoring the bilayer structure factor, we estimate the integrated scattering of the resonance to be $\pi^{-1} \int d\omega \int d^3q [n(\omega) + 1] \chi''(\mathbf{q}, \omega) = 0.052 \mu_B^2$ per formula unit where d^3q is in reciprocal lattice units. Our integrated intensity for the resonance compares very well to the results of previous studies for similar oxygen concentrations. Because of resolution effects, the true comparison between different groups and experiments comes from the integral of χ'' in both momentum and energy. Fong *et al.*⁵⁷ calibrated their measurements using an acoustic phonon and have obtained an integral of $0.069 \mu_B^2$ for YBCO_{6.5}. As noted in the Appendices, the definitions used in that work are identical to the ones used here. Dai *et al.*⁶³ have integrated the resonance to find $\sim 0.06 \mu_B^2$ for YBCO_{6.6}. This calibration was conducted using the *isotropic* Cu²⁺ form factor which, given the \mathbf{Q} position in that experiment, would introduce a small $\sim 5\%$ difference between our measurements. A summary of the absolute measurements of the resonance as a function of T_c is plotted in Fig. 24. The general agreement between all measurements is rea-

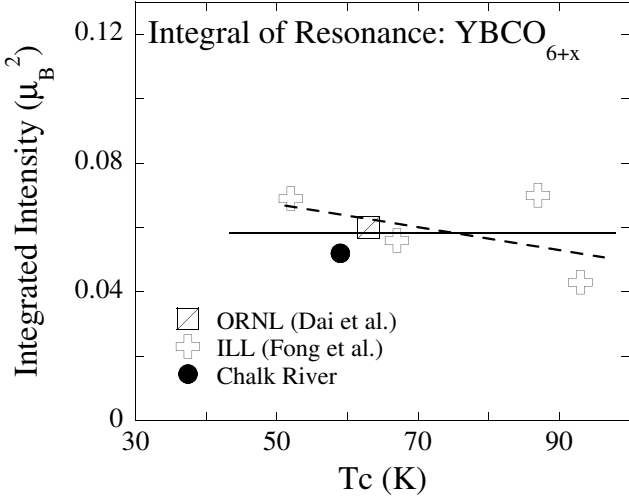


FIG. 24: A summary plot showing the integrated resonance intensity, $\pi^{-1} \int d\omega \int d^3q [n(\omega) + 1] \chi''(\mathbf{q}, \omega)$, measured by several groups for different values of T_c . All measurements have been put on an absolute scale as discussed in the text. This solid line is the average value and the dashed line is a linear fit. An increase of spectral weight with decreasing doping is predicted by both the spin-fermion and SO(5) models.

sonably good. The spectral weight under the resonance can equally well be described as constant (solid line) or as growing, but only slightly, as the doping is reduced (broken line).

An increase in the spectral weight under the resonance peak with decreasing doping is predicted by the SO(5) theory of Demler and Zhang.⁶⁸ Their theory relates the spectral weight in the superconducting state to the difference in exchange energies between the normal and superconducting states extrapolated to $T=0$, taken to be the condensation energy, which is expected to decrease with lower doping. As noted by Demler and Zhang this is consistent with the electronic specific heat measurements of Loram *et al.* who have found a decrease in the condensation energy with decreased doping.⁷⁰ The condensation energy is proportional to the difference in the integral of the dynamic susceptibility. For the spin response below 42 meV we find that in $\text{YBa}_2\text{Cu}_3\text{O}_{6.5}$ the integral $\int d\omega \chi''(\mathbf{q}, \omega)$ (no Bose factor) is indeed larger in the superconducting phase, since it amounts to $17 \pm 2 \mu_B^2$ at 8K and only $13 \pm 2 \mu_B^2$ at 85K, but the difference lies within error.

An increase with reduced doping of the resonance intensity is also a feature of the spin-fermion model.²⁰ With this model, and previous normal state inelastic neutron results, Morr and Pines were able to predict quantitatively a factor of ~ 2 increase in the integrated intensity from optimal doping to $\text{YBCO}_{6.5}$. Our results for ortho-II compared with those of Fong *et al.*⁵⁷ for optimal doping, i.e. the only two systems where a high degree of oxygen order is possible, show that any growth is by a smaller factor.

Ignoring the effect of the chains, and therefore taking only two Cu^{2+} atoms per formula unit, the total spectral weight integrated over all energy and momentum should be given by the total moment sum rule:

$$\int d\omega \int d^3q S(\mathbf{q}, \omega) = 2 \times \frac{2}{3} S (S+1) g^2, \quad (7)$$

where $\int d^3q$ is the momentum space integral over the correlated peak. In this equation the factor of 2 comes from the fact that we are taking two Cu^{2+} ions per formula unit. Here we have assumed that $S(\mathbf{q}, \omega)$ has been corrected for the bilayer structure factor and the Cu^{2+} form factor (see Appendices). We do not expect the total moment sum rule to be strictly obeyed in the superconducting cuprates as the holes will destroy a fraction of the Cu^{2+} moments. Given that the hole doping in our sample is $p \sim 0.1$, this effect should be small and we expect the total measured moment to be similar to that predicted by the sum rule. Equating the above integral to the cross-section for paramagnetic scattering discussed in the Appendices, where the relation between $S(\mathbf{q}, \omega)$ and $\chi''(\mathbf{q}, \omega)$ is defined, we obtain the total moment sum rule for localized spins as the integral over $S(\mathbf{q}, \omega)$:

$$I \equiv \pi^{-1} \int d\omega \int d^3q [n(\omega) + 1] \chi''(\mathbf{q}, \omega) = \frac{2}{3} \mu_B^2 g^2 S(S+1). \quad (8)$$

For $S=\frac{1}{2}$ this gives a total integral of $I=2\mu_B^2$. The resonance in the superconducting state therefore only makes up $\sim 2.6\%$ of the spectral weight predicted by the total moment sum rule. This agrees very well with estimates found in other studies^{17,71} on YBCO_{6+x} and BSCCO_{8+x} . The absolute intensity of the resonance has also been computed from band structure theories and is in reasonably good agreement with our experiment.⁷⁴ Despite the fact that the resonance is strongly affected by the approach and onset of superconductivity, it contributes a tiny fraction of the total moment. Its weakness has led to the suggestion that the presence of a resonance is not crucial to the onset of superconductivity and that it is unlikely the resonance can be associated with the mediating boson of superconductivity.⁷¹ This of course does not exclude the entire high-energy ~ 500 meV spin-wave spectrum from providing the boson, while the resonance is just a redistribution of a tiny fraction of the low-energy spin spectrum in response to the opening of a pairing gap, an idea that we now examine.

To understand the origin of the resonance spectral weight we compare in the superconducting and normal phases the integral from 0 to 42 meV of the two spectra of Fig. 14 multiplied by the Bose factor. The integral, which is equal to $\pi \int d\omega S(\mathbf{q}, \omega)$, was carried out by polynomial interpolation of the data. If the resonance growth has come from energies larger than our 42 meV window,

or from other momenta than than AF region, then we would calculate an increase in the phase. For 8 K we obtained a $\int d\omega \chi''(\mathbf{q}, \omega) [n(\omega) + 1] = 17 \pm 2 \mu_B^2$ and we find $14 \pm 2 \mu_B^2$ for 85 K. Although there is some growth, within error the total weight of the spin correlations is conserved. This indicates that the bulk of the spectral weight gathering at the resonance energy at low temperatures is transferred from from the low-energy incommensurate scattering as this becomes suppressed in the superconducting state. Since the Bose factor increases as $\sim \omega^{-1}$ for small energy transfers, a natural concern with this type of calculation is the weight carried by χ'' at very low energies, a region which is difficult to characterize experimentally. To assess its influence we find that integral from 0 to 5 meV at 85 K amounts to $\sim 0.5 \mu_B^2$, representing only 4% of the total weight. Thus the low-energy limit of χ'' is not contributing a large amount and so validates the accuracy of the integral our finding of a low-energy to resonance transfer.

We now extend our calculations to determine what fraction of the total moment resides in the entire spectrum, not just the part under the resonance. By integrating numerically up to 42 meV, and with the same \mathbf{q} -dependence (Gaussian in the a - b plane and constant along the c direction) we find a total integral of $\pi^{-1} \int d\omega \int d^3q [n(\omega) + 1] \chi''(\mathbf{q}, \omega) \sim 0.06 \mu_B^2$. We conclude that the spin response below 42 meV carries about 3% of the spectral weight available from the total moment sum rule. Thus the spin response below 42 meV captures only a small fraction of the total moment and illustrates the importance of studying higher energy spin fluctuations.

V. DISCUSSION

We first discuss the contribution to the absolute total moment squared of the entire spectrum up to 43 meV. We have shown above that this amounts to $\sim 0.06 \mu_B^2$ per formula unit. For a single Cu^{2+} spin this gives $\sim 0.03 \mu_B^2$, comparable that observed to develop (on cooling in zero field)⁷² in underdoped $\text{La}_{1-x}\text{Sr}_x\text{CuO}_4$ with $x=0.1$, a doping similar to that for the present $\text{YBCO}_{6.5}$. This is one of the many similarities with the LSCO system. We note that both YBCO and YBCO ortho-II exhibit scattering that extends to the lowest energies in the normal phase with incommensurate features characteristic of moving stripes. There is a shorter correlation length in YBCO ortho-II, yet we have shown that the incommensurate wave vector tracks the doping equally in both systems (Fig. 7). For LSCO, if we associate the resonance with the enhanced response at energies above the region where superconductivity suppresses $\chi''(\mathbf{Q}, \omega)$, then qualitatively there is much similar behavior in LSCO and in YBCO.

On cooling below T_c the strong enhancement of spectral weight in the resonance energy region is predicted by band structure calculations based on BCS theory.^{73,74}

The presence of resonance intensity at temperatures above T_c is not.

One aspect of the resonance observed here at high resolution appears different from the results of previous studies of YBCO. Its spectral shape is asymmetric with a sharp drop-off above the peak, and with a much slower decrease along a wing below the resonance. This wing connects smoothly with the previously noted linear, low-energy response part of $\chi''(\mathbf{Q}, \omega)$. Several band calculations⁷⁴ predict the opposite asymmetry as does the t-J model^{75,76}. Norman⁷⁴ has noted that the band calculation for $\chi''(\mathbf{Q}, \omega)$ drops off too fast below the resonance. On the other hand the spin-fermion model of Morr and Pines²⁰ gives a spectral shape for the resonance with a tail to low energies as we observe.

The physical mechanism underlying the resonance peak still remains unknown and a matter of much debate. Band structure calculations using a single band associate the resonance peak with the opening of a superconducting d-wave gap in the excitation spectrum.^{19,58} Since these theories are mean-field they are not able to explain the presence of the resonance in the normal phase at a similar energy to that in the superconducting state. Other theories such as that of Wen and Lee, where d-symmetry normal-phase fluctuations are dynamic,⁹ may be more appropriate. The QED₃ theory, which takes into account vortex-antivortex fluctuations within the pseudogap region, may also account for the resonance we see above T_c .⁷⁸

A heuristic approach to understanding the spectral form of the resonance is to interpret it as the result of a sampling of the density of states of the d-superconducting (dSC) gap function. In this picture the spectral weight of the overdamped low-lying spin response is pushed up to energies above a varying gap function. This accords with our observation of a transfer from low to the resonance energies as superconducting order develops. We find that a uniform sampling of a dSC form of gap function, $\Delta_{\mathbf{k}} = (\Delta_0/2)(\cos(k_x) - \cos(k_y))$ gives a good account of the initial rise in χ'' , and also the cusp-like cut off we observe at the maximum energy of the resonance.⁷⁹ This might suggest that the spins couple to an incoherent charge spectrum so that the momentum conservation between the spin response and charge response of a band model is compromised. It would imply that the cutoff beyond the resonance might be a measure of twice the maximum gap, $2\Delta_0 \sim 33$ meV. However, the recent band theory of Eschrig and Norman⁸⁰, which models the ARPES charge spectrum of $\text{Bi}_2\text{Sr}_2\text{CaCu}_2\text{O}_{8+\delta}$, predicts for $p=0.1$ that the charge pairing gap $2\Delta_M = 120$ meV $\sim 30k_B T_c$ is much larger than the spin resonance energy, $2\Delta_0 \sim 6k_B T_c$, and that it increases while the resonance energy declines with reduced doping. This much larger energy scale presumably provides the less metallic environment in which a spin resonance can survive with relatively little damping. An attractive feature of the model,⁸⁰ however, is that it predicts an increasing degree of incoherence in the charged quasiparticle properties as

doping is reduced, a finding that lends support to the momentum averaging that underlies by our heuristic model.

The sharp cutoff of the resonance at high energies may also be explained by a spin spectrum that has the form of an umbrella in $E - q$ space, as we noted earlier with respect to Batista's work⁶⁶. What happens to the spin-wave branches that do not cross remains an issue. Clearly, there are many possibilities for the origin of the resonance and more experimental work is required to resolve this issue.

We have looked for behavior that might account for the decline on cooling of the NMR relaxation rate $1/T_1T$, which has been associated with a pseudogap temperature of ~ 150 K. We note that the low-energy dynamic susceptibility in the meV range does the opposite - it increases on cooling from room temperature right through the pseudogap range, and continues to rise until interrupted by superconducting pairing below 59 K. Since the normal response below 16 meV is linear in ω , it follows that its slope $\chi''(\mathbf{Q}, \omega)/\omega$, which amounts to $51 \mu_B^2/\text{meV}$ and which is proportional to the NMR relaxation rate $1/T_1T$, also increases while the NMR relaxation decreases. The different temperature dependence of the NMR and neutron spin response, suggests that either the extrapolation from the THz neutron to MHz NMR frequency range is far from linear, or that it is at the other wave vectors sampled by the local NMR probe that the pseudogap suppression takes place.

The only feature in the neutron spin response which has an onset near the presumed pseudogap temperature is the resonance peak which grows in below 170 K. The increasing weight in the resonance may be interpreted in terms of a shift of spectral weight away from very low energies. In comparing the results in the superconducting state with those in the normal phase, we have noted earlier that the rapid increase of the resonance intensity below T_c can be accounted for by the loss of low-energy intensity below $\hbar\omega \sim 20$ meV. Such a picture cannot account for the normal state, where the neutron spin susceptibility inexorably rises on cooling and gathers extra weight at the resonance frequency well above T_c accompanied by growth, rather than suppression at low energies. It is possible that the spectral weight under the normal state resonance may be acquired from higher energies or momenta, well removed from (π, π) . However, since the resonance energy scale is already much larger than thermal energies, it is unlikely that there are substantial changes in the higher energy spectrum near (π, π) . On the other hand, the depression of the local NMR spin susceptibility (Fig. 9), which reflects an average over momenta, suggests that much of the resonance weight is being transferred from low momentum fluctuations.

While the spin correlations at all energies remain visible to the highest temperatures as a single correlated peak at (π, π) , the formation of the stripe modulation only becomes observable below ~ 120 K. This is in a broadly similar temperature range to where we see the

resonance begin to grow in. The emergence of resonance intensity and stripe modulations are associated in the model of Batista *et al.*⁶⁶

Calculations for the 2D Hubbard cluster model⁸¹ also indicate that uniform rather than antiferromagnetic spin fluctuations are causing the pseudogap. However, they find no evidence for pairing fluctuations for $T_c < T < T^*$, and reject the notion of preformed pairs in favor of RVB spin-charge separation. Many of the problems of the single-band theories may indeed be overcome by a theory (such as spin-charge separation) where the dynamics are not described in terms of individual quasiparticles.⁸² Spin-charge separation is also favored in the theory of P. Lee⁶.

In the energy spectrum the pseudogap is clearly seen as noted above in the charge response given by the optical conductivity.^{2,84} For $\text{YBCO}_{6.7}$ the c-axis conductivity is suppressed below an energy of ~ 50 meV. It grows in at high temperatures $\sim 3T_c$. For $\text{YBCO}_{6.6}$ the suppression of the a-b optical conductivity is below 80 meV.² The connection between the resonance in the spin susceptibility and the charge dynamics has been made in the work of Schachinger *et al.* and Carbotte *et al.*^{85,86}

Demler and Zhang⁶⁸ have described in the $\text{SO}(5)$ theory how a particle-particle (p-p) triplet resonance arises from paired carriers. The spin resonance at 33 meV then gives the maximum energy, $2\Delta_0$ to create a pair when the d-wave superconducting (dSC) gap function is $\Delta = (\Delta_0/2)(\cos(k_x) - \cos(k_y))$. The pair resonance can only be seen in neutron scattering when it is coupled to the spin susceptibility by the superconducting order parameter. A reduction of the superconducting order by a magnetic field would then lessen the coupling to the spin channel as found by Dai *et al.*, who observed the resonance intensity to weaken with field.⁸⁷ The triplet symmetry of the $\text{SO}(5)$ spin resonance is confirmed by our polarized neutron results which can be interpreted in terms of a singlet ground state with a triplet excited state. It is more difficult to understand the presence of the spin resonance in the normal phase, albeit weakened but of similar spectral form. Indeed Demler and Zhang note that the $\text{SO}(5)$ resonance should be seen in the superconducting but not in the normal phase above T_c . While our observation of the resonance above T_c does not directly support the $\text{SO}(5)$ model, it is possible that the normal phase fluctuations may be of the correct symmetry to mix the $\text{SO}(5)$ p-p resonance into the spin response spectrum. Because mean field is used for the dSC order parameter, neither the $\text{SO}(5)$ theory nor the various band or spin-fermion models²⁰ couple pairing excitations into the spin susceptibility. However, since the neutron spectrum is independent of the sign of Δ_0 , fluctuations of the gap parameter on a timescale slower than the resonance energy should allow a resonance feature to remain in the normal state. The density of states of the dSC gap function is strongly peaked at its maximum energy, and this characteristic energy can persist in the normal phase. The loss of coherence on heating through the

dSC superconducting transition can occur in the nodal regions, without eliminating the high-energy resonance fluctuations. By contrast in an s-wave superconductor the nodeless order parameter is non-zero everywhere, and the gap function would have to collapse in all directions to effect the transition. Extensions to the SO(5) and other models to treat fluctuations so as to extend their validity to the normal phase would be valuable.

VI. CONCLUSION

We have shown that the antiferromagnetic spin fluctuations in $\text{YBCO}_{6.5}$ ortho-II are gapless, with incommensurate modulation at low energy consistent with dynamic stripes. The spin susceptibility curves upward with energy to a well-defined but asymmetric resonance peak at 33 meV followed by a precipitous cut-off. A weakened image of the resonance is readily observed in the normal phase as a well-defined temporal and spatial structure with an asymmetric spectrum similar to that of the superconducting state. On cooling, the resonance at 33 meV ($\sim 6.5 \text{ k}_B T_c$) and low-energy spin fluctuations strengthen until the superconducting phase at 59 K is reached. As coherent superconducting order is established the resonance accelerates its growth rate, while the low-energy fluctuations below T_c are sharply suppressed but not eliminated as expected for a d-wave gap, and transfer much of their weight to the resonance region. The spin susceptibility, which is confined to nearly antiferromagnetic momenta, shows no evidence for an energy gap in the normal phase, and we suggest that experiments in which a pseudogap suppression is seen sample a range of lower momenta. However we find that the resonance and incommensurate response make their appearance below a temperature $T^* \sim 2-3T_c$ comparable with the pseudogap temperature. The fraction of the low-temperature resonance weight that develops before entering the superconducting phase is surprisingly large. We suggest that this indicates that substantial superconducting pairing fluctuations occur in the normal phase of underdoped $\text{YBCO}_{6.5}$.

Acknowledgments

We have benefited from discussions with S. Kivelson, R. Laughlin, M. R. Norman, I. Affleck, R. A. Cowley, R. Coldea, B. Statt, J.P. Carbotte and L. Taillefer. We are grateful to R. L. Donaberger, L. E. McEwan, A. Cull and M. M. Potter for technical assistance at Chalk River. The work at the University of Toronto and the University of British Columbia was supported by the Natural Sciences and Engineering Research Council (NSERC) of Canada. C. Stock acknowledges a GSSSP supplement from the National Research Council (NRC) of Canada.

VII. APPENDIX A: ABSOLUTE UNITS AND CALIBRATION OF SPECTROMETER

To compare our data with that of other groups and to theory we have put our measurements of $\chi''(\mathbf{Q}, \omega)$ on an absolute scale by comparing the measured magnetic intensity to the integrated intensity of a transverse acoustic phonon near the (0 0 6) Bragg peak, e.g. with $\mathbf{Q} = (0.15, 0.15, 6)$. The use of a phonon from the sample provides a good internal calibration which is independent of errors resulting from impurities or domains which may be an issue with the use of a vanadium standard.

For fixed final energy and counting time determined by the fixed counts in an incident beam monitor whose efficiency varied with incident wave vector as $1/k_0$, the measured intensity, I , is directly proportional to the magnetic or phonon cross-section,

$$I(\mathbf{Q}, \omega) \propto S(\mathbf{Q}, \omega). \quad (9)$$

The constant of proportionality (A) can be determined from the measured integrated intensity, $I(\mathbf{Q}) = \int d\omega I(\mathbf{Q}, \omega)$, of an acoustic phonon. In the long wavelength limit

$$I(\mathbf{Q}) = A \left(\frac{\hbar}{2\omega_p} \right) [1 + n(\omega_p)] |F_N|^2 \frac{Q^2 \cos^2(\beta)}{M} e^{-2W}, \quad (10)$$

where M is the known mass of the unit cell, $e^{-2W} \sim 1$ is the Debye-Waller factor, $[1 + n(\omega)]$ is the Bose factor, $|F_N|^2$ is the static structure factor of the Bragg reflection nearest to where the acoustic phonon is measured, and β is the angle between \mathbf{Q} and the phonon eigenvector. Inserting the measured phonon frequency allows a direct measurement of the calibration factor A and therefore allows any measured intensity to be put on an absolute scale.

For the magnetic scattering we relate the measured scattering to the magnetic correlation function by⁸⁸

$$S(\mathbf{Q}, \omega) = g^2 f^2(\mathbf{Q}) B^2(\mathbf{Q}) \sum_{\alpha\beta} \left(\delta_{\alpha\beta} - \hat{Q}_\alpha \hat{Q}_\beta \right) S_{\alpha\beta}(\mathbf{Q}, \omega). \quad (11)$$

The correlation function is related by the fluctuation dissipation theorem to the imaginary part of the spin susceptibility $\chi(\mathbf{Q}, \omega)$ by

$$S_{\alpha\beta}(\mathbf{Q}, \omega) = \pi^{-1} [n(\omega) + 1] \frac{\chi''_{\alpha\beta}(\mathbf{Q}, \omega)}{g^2 \mu_B^2}. \quad (12)$$

Since the paramagnetic scattering is isotropic in spin, $\chi'' = \chi''_{xx} = \chi''_{yy} = \chi''_{zz}$, we can extract $\chi''(\mathbf{Q}, \omega)$ from the measured intensity, I , through the equation

$$I(\mathbf{Q}, \omega) = A \frac{(\gamma r_o)^2}{4} f^2(\mathbf{Q}) B^2(Q_z) e^{-2W} \frac{[1 + n(\omega)]}{\pi \mu_B^2} (2\chi''(\mathbf{Q}, \omega)). \quad (13)$$

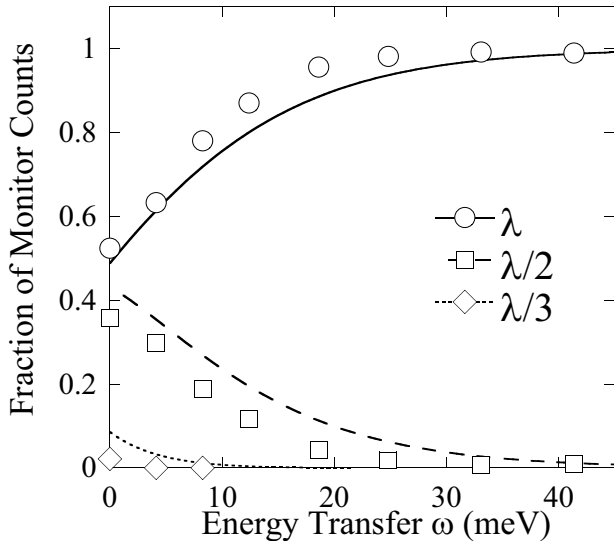


FIG. 25: The fraction of neutrons hitting the diffracted beam monitor is plotted as a function of energy transfer for $\lambda/n = \lambda/1, \lambda/2$, and $\lambda/3$. The final energy is taken to be 14.5 meV where then energy transfer is defined as $\hbar\omega = E_i - E_f$. The solid curves are calculations using a Maxwellian distribution and a moderator temperature $k_B T = 28.8$ meV.

The factor 2 comes from the Lorentz factor and χ'' denotes the susceptibility per formula unit here and in the body of paper. We have chosen to use the anisotropic form factor $f^2(\mathbf{Q})$ over the isotropic form⁸⁹ because the anisotropic form has been carefully verified in the ordered antiferromagnetic system and in the Al doped YBCO system.^{90,91} For practical cross-section calculations $\frac{(\gamma\tau_0)^2}{4}$ is 73 mbarns sr^{-1} . The paramagnetic description for the spin scattering follows from our polarized measurements and from our studies of the Lorentz factor in different Brillouin zones. These show no preferred polarization of the fluctuations. The factor $B(Q_z)$ is the bilayer structure factor equal to $\sin(Q_z d/2)$, where d is the intrabilayer spacing. In the normalization to absolute units of the spin fluctuations below ~ 40 meV energy transfers we have only considered the acoustic, or odd, fluctuations to the susceptibility since these predominate at the momenta studied. In the notation of Fong *et al.* we have calculated $\chi_{odd}''(\mathbf{Q}, \omega)$ only.

The definitions of the magnetic cross-section used here are identical to those used in the phonon calibration by Fong *et al.*⁵⁷ The vanadium calibrations conducted by Dai *et al.*⁶³ use the isotropic form factor but otherwise the same equations were used⁹² as presented here. This allows a direct comparison between different experiments.⁹³

VIII. APPENDIX B: CORRECTION FOR HIGHER ORDER CONTAMINATION OF MONITOR

The low-efficiency fission monitor in the incident beam only approximately removes the factor $1/k_0$ from the measure cross-section. As the incident energy decreases, the monitor rate is perturbed because it senses an increasing fraction of higher-order neutrons reflected by the monochromator out of the reactor spectrum. Thus low-energy transfer scattering would be underestimated if no correction were made. To understand the relative intensities as a function of energy transfer, a complete characterization and correction for this contamination is essential.

We determined the relative weight of $\lambda/2$ and $\lambda/3$ neutrons over the energy range of our experiments from the relative intensities of aluminum powder Bragg peaks in two-axis mode. The relative flux of each component of the incident beam can be uniquely calculated from the following formula⁹⁴,

$$I(2\theta) \propto \Phi(\lambda) \frac{\lambda^3}{\sin(2\theta) \sin(\theta)} \sum_{\mathbf{Q}} |F_N(\mathbf{Q})|^2 \quad (14)$$

where Φ is the incident flux, $|F_N(\mathbf{Q})|^2$ is the nuclear structure factors and the sum is over constant $|\mathbf{Q}|$.

By correcting for the $1/k_0$ monitor efficiency the relative fraction of monitor counts in the beam from λ , $\lambda/2$, and $\lambda/3$ orders were calculated as shown in Fig. 25. We also computed the fractions for a Maxwellian distribution of neutrons, a moderator temperature of $kT = 28.8$ meV (60°C), and for these three components only. The resultant fraction of each order is⁹⁵

$$F(n^2, E_i) = \frac{(n^2) e^{-(n^2 E_i)/kT}}{e^{-E_i/kT} + 4e^{-4E_i/kT} + 9e^{-9E_i/kT}}. \quad (15)$$

As shown for $n = 1, 2$, and 3 in Fig. 25 this simple model provides a reasonable description of the data given that we have not corrected for the energy dependent reflectivity of the monochromator. As can be seen from Fig. 25 the correction factor required for low energies is substantial. Inclusion of this factor is essential for obtaining an accurate form for the spectral distribution, as we have done from 0 to 43 meV. The correction becomes particularly important when discussing low-energy excitations where it amounts to a factor two. Neglect of the factor would make it more difficult to observe low-energy scattering and might lead to an inference that a normal state spin gap was present.

¹ M.A. Kastner, R.J. Birgeneau, G. Shirane, and Y. Endoh, Rev. Mod. Phys. **70**, 897 (1998).

² T. Timusk and B.W. Statt, Rep. Prog. Phys. **62**, 61 (1999).

³ Ch. Renner, B. Revaz, J.-Y. Genoud, K. Kadokawa, and O. Fischer, Phys. Rev. Lett. **80**, 149 (1998).

⁴ W.W. Warren, Jr., R.E. Walstedt, G.F. Brennert, R.J. Cava, R. Tycko, R.F. Bell, and G. Dabbagh, Phys. Rev. Lett. **62**, 1193 (1989).

⁵ H. Yasuoka, Physica C **282-287**, 119 (1997).

⁶ P.A. Lee, Physica C **317-318**, 194 (1999).

⁷ P.A. Lee, unpublished (cond-mat/0201052).

⁸ C.M. Varma, Phys. Rev. B **55**, 14554 (1997).

⁹ X.-G. Wen and P.A. Lee, Phys. Rev. Lett. **76**, 503 (1996).

¹⁰ S. Chakravarty, H.-Y. Kee, C. Nayak, Int. J. Mod. Phys. B **15**, 2901 (2001); S. Chakravarty, R. B. Laughlin, D. K. Morr, and C. Nayak, Phys. Rev. B **63**, 094503 (2001)

¹¹ S.A. Kivelson, E. Fradkin, and V.J. Emery, Nature **393**, 550 (1998).

¹² V.J. Emery, S.A. Kivelson, and O. Zachar, Phys. Rev. B **56**, 6120 (1997).

¹³ S.A. Kivelson, E. Fradkin, V. Oganesyan, I.P. Bindloss, J.M. Tranquada, A. Kapitulnik, and C. Howald, unpublished (cond-mat/0210683).

¹⁴ S. Wakimoto, R.J. Birgeneau, M.A. Kastner, Y.S. Lee, R. Erwin, P.M. Gehring, S.H. Lee, M. Fujita, K. Yamada, Y. Endoh, K. Hirota, and G. Shirane, Phys. Rev. B **61**, 3699 (2000).

¹⁵ H.A. Mook, P. Dai, F. Dogan, and R.D. Hunt, Nature **404**, 729 (2000).

¹⁶ H.A. Mook, M. Yethiraj, G. Aeppli, T.E. Mason, T. Armstrong, Phys. Rev. Lett. **70**, 3490 (1993).

¹⁷ B. Keimer, P. Bourges, H.F. Fong, Y. Sidis, L.P. Regnault, A. Ivanov, D.L. Milius, I.A. Aksay, G.D. Gu, and N. Koshizuka, J. Phys. Chem. Solids **60**, 1007 (1999).

¹⁸ H. He, P. Bourges, Y. Sidis, C. Ulrich, L.P. Regnault, S. Pailhes, N.S. Berzigiarova, N.N. Kolesnikov, and B. Keimer, Science **295**, 1045 (2002).

¹⁹ M.R. Norman, Phys. Rev. B **63**, 092509 (2001).

²⁰ D.K. Morr and D. Pines, Phys. Rev. Lett. **81**, 1086 (1998).

²¹ J.L. Tallon, C. Bernhard, H. Shaked, R.L. Hitterman, and J.D. Jorgensen, Phys. Rev. B **51**, R12911 (1995).

²² J.D. Jorgensen, B.W. Veal, A.P. Paulikas, L.J. Nowicki, G. W. Crabtree, H. Claus, and W.K. Kwok, Phys. Rev. B **41**, 1863 (1990).

²³ H. Casalta, P. Schleger, P. Harris, B. Lebech, N.H. Andersen, R. Liang, P. Dosanjh, and W.N. Hardy, Physica C **258**, 321 (1996).

²⁴ D. Peets, R. Liang, C. Stock, W. J. L. Buyers, Z. Tun, L. Taillefer, R. J. Birgeneau, D. Bonn, and W. N. Hardy, J. Supercond. **15**, 531 (2002).

²⁵ C. Stock, W.J.L. Buyers, Z. Tun, R. Liang, D. Peets, D. Bonn, W.N. Hardy, and L. Taillefer, Phys. Rev. B **66**, 024505 (2002).

²⁶ N.H. Andersen, M.von Zimmermann, T. Frello, M. Kall, D. Monster, P.-A. Lindgard, J. Madsen, T. Niemoller, H.F. Poulsen, O. Schmidt, J.R. Schneider, Th. Wolf, P. Dosanjh, R. Liang, and W.N. Hardy, Physica C **317-318**, 259 (1999) found $\xi_a=50$ Å.

²⁷ R. Liang, D.A. Bonn, and W.N. Hardy, Physica C **336**, 57 (2000) found $\xi_a=148$ Å.

²⁸ R.M. Moon, T. Riste, and W.C. Koehler, Phys. Rev. **181**, 920 (1969).

²⁹ P. Dai, H.A. Mook, R.D. Hunt, and F. Dogan, Phys. Rev. B **63**, 054525 (2001).

³⁰ Y.-W. Hsueh, B.W. Statt, M. Reedyk, J.S. Xue, and J.E. Greidan, Phys. Rev. B **56**, 8511 (1997).

³¹ Y. Itoh, T. Machi, A. Fukuoka, K. Tanabe, and H. Ya- suoka, J. Phys. Soc. Jpn. **65**, 3751 (1996).

³² S. Fujiyama, Y. Itoh, H. Yasuoka, and Y. Ueda, J. Phys. Soc. Jpn. **66**, 2864 (1997).

³³ C.H. Lee, K. Yamada, H. Hiraka, C.R. Venkateswara, and Y. Endoh, unpublished (cont-mat/0209225).

³⁴ H. Chou, J.M. Tranquada, G. Shirane, T.E. Mason, W.J.L. Buyers, S. Shamoto, and M. Sato, Phys. Rev. B **43**, 5554 (1991).

³⁵ B.J. Sternlieb, G. Shirane, J.M. Tranquada, M. Sato, and S. Shamoto, Phys. Rev. B **47**, 5320 (1993).

³⁶ R.J. Birgeneau, R.W. Erwin, P.M. Gehring, M.A. Kastner, B. Kiemer, M. Sato, S. Shamoto, and G. Shirane, Z. Phys. B **87**, 15 (1992).

³⁷ J.M. Tranquada, B.J. Sternlieb, J.D. Axe, Y. Nakamura, and S. Uchida, Nature **375**, 561-563 (1995).

³⁸ Throughout this paper we use \mathbf{Q} to refer to a Bragg peak or the (π, π) position and \mathbf{q} is taken with respect to \mathbf{Q} .

³⁹ M. Arai, T. Nishijima, Y. Endoh, T. Egami, S. Tajima, K. Tomimoto, Y. Shiohara, M. Takahashi, A. Garrett, and S.M. Bennington, Phys. Rev. Lett. **83** 608 (1999).

⁴⁰ J.M. Tranquada, Physica C **282-287** 166 (1997).

⁴¹ D.K. Morr, J. Schmalian and D. Pines, unpublished (cond-mat/0002164).

⁴² O. K. Andersen, O. Jepsen, A. I. Liechtenstein, and I. I. Mazin, Phys. Rev. B. **49**, 4145 (1994).

⁴³ S. Kivelson, (private communication).

⁴⁴ K. Yamada, C.H. Lee, K. Kurahashi, J. Wada, S. Wakimoto, S. Ueki, H. Kimura, Y. Endoh, S. Hosoya, G. Shirane, R.J. Birgeneau, M. Greven, M.A. Kastner, and Y.J. Kim, Phys. Rev. B **57** 6165 (1998).

⁴⁵ A.V. Balatsky and P. Bourges, Phys. Rev. Lett. **82**, 5337 (1999).

⁴⁶ D.J. Derro, E.W. Hudson, K.M. Lang, S.H. Pan, J.C. Davis, J.T. Markert, and A.L. de Lozanne, Phys. Rev. Lett. **88**, 097002 (2002).

⁴⁷ B. Keimer, R.J. Birgeneau, A. Cassanho, Y. Endoh, R.W. Erwin, M.A. Kastner, and G. Shirane, Phys. Rev. Lett. **67**, 1930 (1991).

⁴⁸ H. Hiraka, Y. Endoh, M. Fujita, Y.S. Lee, J. Kulda, A. Ivanov, and R.J. Birgeneau, J. Phys. Soc. Jpn. **70**, 853 (2001).

⁴⁹ C.M. Varma, P.B. Littlewood, S. Schmitt-Rink, E. Abrahams, and A.E. Ruckenstein, Phys. Rev. Lett. **63**, 1996 (1989).

⁵⁰ J. Zaanen and W.van Saarloos, Physica C **282-287**, 178 (1997).

⁵¹ M. Matsuda, R.J. Birgeneau, Y. Endoh, Y. Hidaka, M.A. Kastner, K. Nakajima, G. Shirane, T.R. Thurston, and K. Yamada, J. Phys. Soc. Jpn. **62**, 1702 (1993).

⁵² G. Aeppli, T.E. Mason, S.M. Hayden, H.A. Mook, and J. Kulda, Science **278**, 1432 (1997).

⁵³ C.M. Varma, Phys. Rev. Lett. **83**, 3538 (1999).

⁵⁴ P.M. Gehring, J.M. Tranquada, G. Shirane, J.R.D. Copley, R.W. Erwin, M. Sato, and S. Shamoto, Phys. Rev. B **44**, 2811 (1991).

⁵⁵ K. Yamada, S. Wakimoto, G. Shirane, C.H. Lee, M.A. Kastner, S. Hosoya, M. Greven, Y. Endoh, and R. J. Birgeneau, Phys. Rev. Lett. **75**, 1626 (1995).

⁵⁶ B. Lake, G. Aeppli, T.E. Mason, A. Schröder, D.F. Morrow, K. Lefmann, M. Isshiki, M. Nohara, H. Takagi, and S.M. Hayden, Nature **400**, 43 (1999).

⁵⁷ H.F. Fong, P. Bourges, Y. Sidis, L.P. Regnault, J. Bossy, A. Ivanov, D.L. Milius, I.A. Aksay, and B. Keimer, Phys. Rev. B **61**, 14773 (2000).

⁵⁸ N. Bulut and D.J. Scalapino, Phys. Rev. B **47**, 3419 (1993).

⁵⁹ P. Bourges, Y. Sidis, H.F. Fong, L.P. Regnault, J. Bossy, A. Ivanov, and B. Keimer, Science **288**, 1234 (2000).

⁶⁰ L.P. Regnault, P. Bourges, P. Burlet, J.Y. Henry, J. Rossat-Mignod, Y. Sidis, and C. Vettier, Physica B **213-214**, 48 (1995).

⁶¹ P. Bourges, H.F. Fong, L.P. Regnault, J. Bossy, C. Vettier, D.L. Milius, I.A. Aksay and B. Keimer, Phys. Rev. B **56**, R11439 (1997).

⁶² S.M. Hayden, G. Aeppli, H.A. Mook, T.G. Perring, T.E. Mason, S.-W. Cheong, and Z. Fisk, Phys. Rev. Lett. **76**, 1344 (1996).

⁶³ P. Dai, H.A. Mook, S.M. Hayden, G. Aeppli, T.G. Perring, R.D. Hunt, and F. Dogan, Science **284**, 1344 (1999).

⁶⁴ S.-C. Zhang, Science **275**, 1089 (1997).

⁶⁵ M. Fujita, K. Yamada, H. Hiraka, P.M. Gehring, S.H. Lee, S. Wakimoto, and G. Shirane, Phys. Rev. B **65**, 064505 (2002).

⁶⁶ C.D. Batista, G. Ortiz, and A.V. Balatsky, Int. J. Mod. Phys. B **14**, 3334 (2000).

⁶⁷ G. Ortiz, C.D. Batista, and A.V. Balatsky, Physica C **364-365**, 549 (2001).

⁶⁸ E. Demler and S.-C. Zhang, Nature **396**, 733 (1998).

⁶⁹ H.F. Fong, B. Keimer, D. Reznik, D.L. Milius, and I.A. Aksay, Phys. Rev. B **54**, 6708 (1996).

⁷⁰ J.W. Loram, K.A. Mirza, J.R. Cooper, and J.L. Tallon, Physica C **282-287**, 1405 (1997).

⁷¹ H.-Y. Kee, S.A. Kivelson, and G. Aeppli, Phys. Rev. Lett. **88**, 257002 (2002).

⁷² B. Lake, H.M. Ronnow, N.B. Christensen, G. Aeppli, K. Lefmann, D.F. McMorrow, P. Vorderwisch, P. Smeibidl, N. Mangkorntong, T. Sasagawa, M. Nohara, H. Takagi and T.E. Mason, Nature **415**, 299 (2002).

⁷³ N. Bulut and D.J. Scalapino, Phys. Rev. B **53**, 5149 (1996).

⁷⁴ M.R. Norman, Phys. Rev. B **61**, 14751 (2000).

⁷⁵ T. Tanamoto, H. Kohno, and H. Fukuyama, J. Phys. Soc. Jpn. **63**, 2739 (1994).

⁷⁶ J. Brinckmann and P.A. Lee, Phys. Rev. Lett. **82**, 2915 (1999).

⁷⁷ P. Bourges, L.P. Regnault, J.Y. Henry, C. Vettier, Y. Sidis, and P. Burlet, Physica B **215**, 30 (1995).

⁷⁸ M. Franz, Z. Tesanovic, and O. Vafek, Phys. Rev. B **66**, 054535 (2002).

⁷⁹ The dSC density of states of the gap function, folded with the resolution, is used rather than the single particle density of states of F. Marsiglio, Phys. Rev. **47**, 5419 (1993), which would give a similar asymmetry.

⁸⁰ M. Eschrig and M.R. Norman, Phys. Rev. B **67**, 144503 (2003).

⁸¹ Th.A. Maier, M. Jarrell, A. Macridin, and F.-C. Zhang, unpublished (cond-mat/0208419).

⁸² P.W. Anderson, Physica C **341-348**, 9 (2000).

⁸³ M.C. Schabel, C.-H. Park, A. Matsuura, Z.-X. Shen, D.A. Bonn, R. Liang, and W.N. Hardy, Phys. Rev. B **57**, 6107 (1998).

⁸⁴ C.C. Homes, T. Timusk, R. Liang, D.A. Bonn and W.N. Hardy, Phys. Rev. Lett. **71**, 1645 (1993).

⁸⁵ E. Schachinger, J.P. Carbotte, and D.N. Basov, Europhys. Lett. **54**, 380 (2001).

⁸⁶ J.P. Carbotte, E. Schachinger, and D.N. Basov, Nature **401**, 354 (1999).

⁸⁷ P. Dai, H.A. Mook, G. Aeppli, S.M. Hayden, F. Dogan, Nature **406**, 965 (2000).

⁸⁸ W.J.L. Buyers and T.M. Holden, Handbook on the Physics and Chemistry of the Actinides, eds. A.J. Freeman and G.H. Lander, Elsevier (1985) page 239

⁸⁹ R.E. Watson and R.J. Freeman, Acta. Cryst. **14**, 27 (1961).

⁹⁰ S. Shamoto, M. Sato, J.M. Tranquada, B.J. Sternlieb, and G. Shirane, Phys. Rev. B **48**, 13817 (1993).

⁹¹ E. Brecht, W.W. Schmahl, H. Fuess, H. Casalta, P. Schleger, B. Lebech, N.H. Andersen, and Th. Wolf, Phys. Rev. B **52**, 9601 (1995).

⁹² S.M. Hayden, G. Aeppli, P. Dai, H.A. Mook, T.G. Perring, S.-W. Cheong, Z. Fisk, F. Dogan, and T.E. Mason, Physica B **241-243**, 765 (1998).

⁹³ The work by Dai *et al.* and Fong *et al.* contain an extra factor of $1/g^2$ but do not include the factor of $1/4$ in front of the (γr_0) term. Since $g=2$ these two definitions are equivalent.

⁹⁴ G. L. Squires, *Introduction to Thermal Neutron Scattering* (Dover Publications, New York, 1996).

⁹⁵ G. E. Bacon, *Neutron Diffraction* (Oxford University Press, London, 1962).